Food & Function

ROYAL SOCIETY OF CHEMISTRY

PAPER

View Article Online
View Journal | View Issue

Cite this: *Food Funct.*, 2023, **14**, 8291

Pterostilbene alleviated cerebral ischemia/reperfusion-induced blood–brain barrier dysfunction *via* inhibiting early endothelial cytoskeleton reorganization and late basement membrane degradation†

Zhi-hong Yang,‡[a] Ye-ju Liu,‡[a] Wei-kang Ban,[a] Hai-bo Liu,[a] Ling-juan Lv,[a] Bao-yue Zhang,[c] Ai-lin Liu,[c] Zi-yu Hou,[a] Juan Lu,[a] Xi Chen[a] and Yu-yang You*[b]

Pterostilbene, an important analogue of the star molecule resveratrol and a novel compound naturally occurring in blueberries and grapes, exerts a significant neuroprotective effect on cerebral ischemia/reperfusion (I/R), but its mechanism is still unclear. This study aimed to follow the molecular mechanisms behind the potential protective effect of pterostilbene against I/R induced injury. For fulfilment of our aim, we investigated the protective effects of pterostilbene on I/R injury caused by middle cerebral artery occlusion (MCAO) *in vivo* and oxygen-glucose deprivation (OGD) *in vitro*. Machine learning models and molecular docking were used for target exploration and validated by western blotting. Pterostilbene significantly reduced the cerebral infarction volume, improved neurological deficits, increased cerebral microcirculation and improved blood–brain barrier (BBB) leakage. Machine learning models confirmed that the stroke target MMP-9 bound to pterostilbene, and molecular docking demonstrated the strong binding activity. We further found that pterostilbene could depolymerize stress fibers and maintain the cytoskeleton by effectively increasing the expression of the non-phosphorylated actin depolymerizing factor (ADF) in the early stage of I/R. In the late stage of I/R, pterostilbene could activate the Wnt pathway and inhibit the expression of MMP-9 to decrease the degradation of the extracellular basement membrane (BM) and increase the expression of junction proteins. In this study, we explored the protective mechanisms of pterostilbene in terms of both endothelial cytoskeleton and extracellular matrix. The early and late protective effects jointly maintain BBB stability and attenuate I/R injury, showing its potential to be a promising drug candidate for the treatment of ischemic stroke.

Received 30th June 2023,
Accepted 31st July 2023

DOI: 10.1039/d3fo02639f

rsc.li/food-function

1. Introduction

Stroke has become the second leading cause of death in the world.[1] It is characterized by high incidence, recurrence rate, disability rate and mortality rate, which has brought a heavy burden to society and families. Ischemic stroke is the most common type of stroke, accounting for about 87% of all stroke cases.[2] Recombinant tissue plasminogen activator (tPA) is the only drug approved by the FDA for thrombolytic therapy in the treatment of ischemic stroke, but only a few patients can benefit from this treatment due to the risks of hemorrhage transformation (HT)[3] and a narrow time window.[4] In recent years, the development of safe and effective drugs with multiple targets and clear mechanisms has become a research focus due to the difficulty in ischemic stroke treatment.[5]

The series of neurochemical processes involved in cerebral ischemia is called the ischemic cascade. In the ischemic cascade, blood–brain barrier (BBB) dysfunction can persist from hours up to weeks.[6] Early BBB permeability may be partially reversible,[7] making it a reasonable target for therapeutic intervention. Brain microvascular endothelial cells (BMECs), as the basic structure and main component of the BBB, are important for maintaining the integrity and permeability of the BBB. There are continuous intercellular junctions between

[a]*Institute of Medicinal Plant Development, Chinese Academy of Medical Sciences and Peking Union Medical College, Beijing 100193, China. E-mail: zhyang@implad.ac.cn, yejuliu@126.com*
[b]*Beijing Institute of Technology, Beijing 100081, China. E-mail: youyuyang@bit.edu.cn; Tel: +86-10-5755-4665*
[c]*Institute of Materia Medica, Chinese Academy of Medical Sciences and Peking Union Medical College, Beijing 100050, China*

†Electronic supplementary information (ESI) available. See DOI: https://doi.org/10.1039/d3fo02639f

‡These authors contributed equally to this work.

BMECs, including tight junctions (TJs) and adherens junctions (AJs). The TJ proteins (occludin and claudin) and the AJ protein (VE-cadherin) are in turn anchored to the intracellular actin cytoskeleton by multiple accessory proteins (*e.g.*, zonula occludens) to maintain dynamic structures.[8] Previous studies have shown that BMEC actin polymerizes into linear stress fibers under hypoxic conditions. This formation of stress fibers accompanied by actomyosin contraction and increased cytoskeletal tension, leading to cell morphology contraction and TJ damage, ultimately results in hyperpermeability.[9–11] In addition, the specialized extracellular matrix (ECM) of the basement membrane (BM) connects endothelial cells to neighboring cells, such as astrocytes and pericytes, and the molecular components of ECM secreted by them provide important clues to the TJ assembly that maintains mature BBB function.[12] The cytoskeleton of BMECs and intercellular junction proteins, as well as the extracellular BM and ECM jointly maintain the integrity of the BBB and play an irreplaceable role. Therefore, specific interventions based on the above characteristics of BMECs may provide an innovative therapeutic strategy for brain protection against cerebral ischemic injury. As a highly conserved intracellular communication system,[13] the Wnt signaling pathway plays a crucial role in cerebrovascular development and BBB formation.[14–16] Specifically, the classic Wnt/β-catenin pathway is responsible for inducing and maintaining BBB properties throughout an organism's lifespan.[17] Dysregulation of this pathway has been linked to BBB disruption during ischemia-reperfusion events,[18] while activation of the same pathway can protect against such dysfunction.[19]

Dl-3-*n*-butylphthalide (NBP) was first discovered in the seeds of *Apium graveolens* Linn. and was approved as an anti-ischemic stroke drug by the National Medical Products Administration of China in 2002.[20] Several studies have confirmed that NBP can reduce cerebral ischemic injury through a variety of mechanisms, the most important of which is to improve cerebral microcirculatory blood flow in the acute phase.[21,22] As the anti-ischemic mechanisms of marketed drugs became clearer, researchers have further explored more compounds with similar effects. In recent years, the study of resveratrol as the primary active ingredient of Resina Draconis for cerebral ischemia has been a hot topic, and significant breakthroughs have been achieved.[23–25] However, resveratrol does not easily cross the BBB and has low oral bioavailability, which are the main limiting factors for its potential clinical application.[26] Pterostilbene (3,5-dimethoxy-4′-hydroxystilbene), an analogue of resveratrol (3,4′,5-trihydroxystilbene), is the primary active ingredient of Resina Draconis, as well as a naturally novel component found in blueberries and grapes in the early 21st century (Fig. 1A).[27,28] The pterostilbene content varies from different types of berries, with 99 ng g^{-1} dry sample in *Vaccinium ashei* (rabbiteye blueberry) and 560 ng g^{-1} dry sample in *Vaccinium stamineum* (deerberry).[29,30] It became a star molecule due to its anti-inflammatory,[31,32] antioxidant,[33,34] anti-tumor,[35–37] neuroprotective,[38–40] lipid-lowering,[41–43] and hypoglycemic[44,45] pharmacological activities, and is called next generation resveratrol. As a structural analog, pterostilbene has better BBB permeability because the substitution of the methoxy group for the hydroxyl group increases its lipid solubility.[46] Several studies have also shown that pterostilbene is more easily absorbed and has good bioavailability and metabolic stability compared with resveratrol.[47,48] It is concluded that pterostilbene may also have a good therapeutic effect on cerebral ischemia.

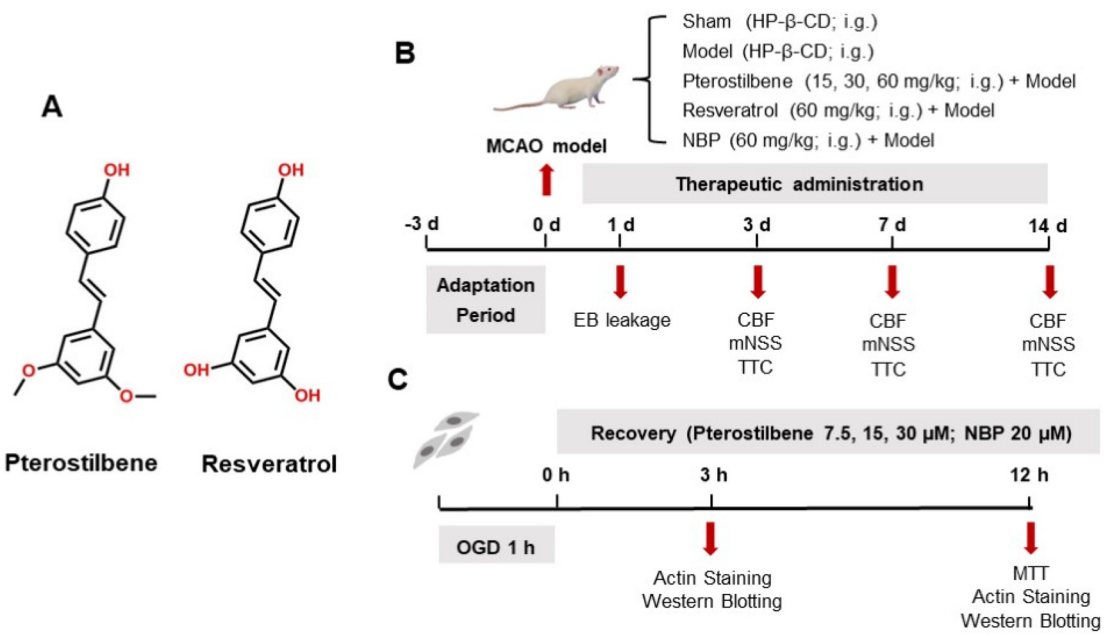

Fig. 1 Chemical structure of pterostilbene and resveratrol and the schematic diagram of the experimental protocols. (A) Chemical structure of pterostilbene and resveratrol. (B and C) Schematic diagram of the experimental protocols *in vivo* (B) and *in vitro* (C).

In the present study, middle cerebral artery occlusion (MCAO) and oxygen-glucose deprivation (OGD) models were used to evaluate the protective effect of pterostilbene on cerebral ischemia *in vivo* and *in vitro*, respectively. Combined with computer-aided methods, we took BMECs as a starting point to explore the potential mechanism of pterostilbene protection against the BBB in terms of the cytoskeleton and extracellular matrix.

2. Materials and methods

2.1 Experimental animals

Male Sprague-Dawley rats (280–300 g) were purchased from Beijing Vital River Experimental Animal Co., Ltd (Beijing, China; certificate No. SCXK2019-0008). The animal care and experimental procedures were approved by the Ethics Committees of the Institute of Medicinal Plant Development, Chinese Academy of Medical Sciences and Peking Union Medical College. Before experimentation, the rats were allowed to acclimatize to the experimental conditions (temperature of 23 ± 1 °C, relative humidity of 55% ± 5%, and a 12 h light–dark cycle) for 3 days and randomly assigned to different groups. Laboratory chow and tap water were provided *ad libitum*.

2.2 Rat MCAO model

In this study, an experimental model of cerebral I/R injury was induced in rats by middle cerebral artery occlusion (MCAO). The surgical procedure was performed according to a previous study.[49] At the beginning of the surgery, it was ensured that the animals in each group were of the same age and of similar weight. In brief, after anesthetization with 10% urethane (i.p., 10 mL kg^{-1}), the right common carotid artery (CCA), external carotid artery (ECA), and internal carotid artery (ICA) were fully exposed. A monofilament with a silicon-coated tip (diameter of 0.38 mm) was inserted into the ICA, advanced to the origin of the middle cerebral artery (MCA) and left in place for 1.5 h. The monofilament was pulled out after 1.5 h of occlusion for reperfusion, and the treatment groups were gavaged accordingly after 1 h of reperfusion. The rats in the sham group underwent the same surgical procedure except for the insertion of the monofilament. The post-operative animals were further housed in groups of 3–4 animals in one cage, and provided with chow and tap water *ad libitum*.

2.3 Experimental groups and drugs

Pterostilbene (purity > 98% by HPLC) and resveratrol (purity > 99% by HPLC) were purchased from Shanghai Bide Pharmaceutical Technology Co., Ltd (Shanghai, China) and dissolved in normal saline containing ten-fold hydroxypropyl-β-cyclodextrin (HP-β-CD). The positive drug NBP was obtained from CSPC-NBP Pharmaceutical Co., Ltd (Hebei, China), and dissolved in normal saline. The animals were randomly divided into the following groups: the sham operation group, model group, pterostilbene + model group, resveratrol + model group, and NBP + model group. The pterostilbene groups were treated with pterostilbene at the dose of 15, 30 and 60 mg kg^{-1} and the resveratrol and NBP groups with 60 mg kg^{-1} pterostilbene were administered by gavage once a day after reperfusion for 1, 3, 7 and 14 days, while the animals in the sham and model groups received the same volume of normal saline containing HP-β-CD. A schematic diagram of the experimental protocols is shown in Fig. 1B.

2.4 Laser speckle imaging technique

Cerebral microcirculatory blood flow (CBF) was monitored using the laser speckle technique. Briefly, a CCD camera (PeriCam PSI System, Perimed, Sweden) was positioned 10 cm above the head, and a laser diode (785 nm) illuminated the intact skull surface, allowing penetration of the laser in a diffuse manner through the brain. The speckle contrast which was derived from the speckle visibility relative to the velocity of the light-scattering particles (blood) was used to measure CBF. Laser speckle images were obtained before MCAO, after blocking MCA and after reperfusion.

2.5 Modified neurological severity score (mNSS) test

Neurological functions, including motor and sensory abilities, were measured by the mNSS test with scores ranging from 0 to 14 (1–4: mild injury, 5–9: moderate injury and 10–14: severe injury) (see ESI Table 1†).[50] Higher scores indicated greater severity of injury. Rat with scores in the range of 5–14 at 24 h after cerebral I/R injury were used for further experiments. Rats in each group were scored at 3, 7 and 14 days after cerebral I/R injury, respectively.

2.6 2,3,5-Triphenyltetrazolium chloride staining

To assess the infarct volume, we performed 2,3,5-triphenyltetrazolium chloride (TTC; Solarbio, Beijing, China) staining. Brains were sliced into five coronal sections and incubated in 2% TTC for 15 min at 37 °C in the dark, and fixed in 4% paraformaldehyde (PFA; Biosharp, Beijing, China) overnight. The area of infarction was quantified, and the infarct volume was calculated using ImageJ software.

2.7 Evans blue leakage assay

At 24 h after cerebral I/R injury, 2% Evans blue dye (EB; Macklin, Shanghai, China) dissolved in normal saline was intravenously injected (0.4 mL per 100 g) into the tail vein and allowed to circulate for 3 h. The left ventricles of the rats were then perfused with heparinized saline until a colorless perfusate was obtained from the right atrium. The brains were isolated, sliced, photographed, weighed and homogenized in dimethylformamide (100 mg per 1 mL). After 24 h in a 60 °C water bath, the samples were centrifuged at 4000 rpm for 20 min. 200 μL of the supernatant was collected, and the absorbance was measured at 620 nm.

2.8 Machine learning model

In this study, we established a machine learning model to predict the potential targets of pterostilbene in the treatment

of cerebral ischemia. Phase 3 and marketed stroke drugs were searched in Thomson Reuters Integrity and TTD databases, and drug targets were further scanned to identify stroke-related targets.[51–53] Then, the known active compounds of the target were searched in the Binding Database. Then, naive Bayes[54] and recursive separation[55] algorithms were used to build the model on a Discovery Studio 2018 platform based on ECFP_6[56] and MACCS[57] molecular fingerprints and descriptors. We carried out five-fold cross-validation of the training set[58] to evaluate the predictive ability of the constructed model.

Pterostilbene, a stilbene compound with two methoxy and one hydroxyl groups, was inputted into the established machine learning model to predict its potential targets for the treatment of stroke. For the machine learning model, the prediction was TRUE or FALSE, with TRUE indicating that the compound can interact with the target and FALSE the opposite.

2.9 Molecular docking

In this study, we performed molecular docking to validate the predicted potential target of pterostilbene. The 2D structure of the small molecule pterostilbene was first drawn using Marvin Sketch software, and the low-energy 3D conformation of the small molecule was obtained by protonation and energy optimization in MOE V2020.09011 to function as the ligand for molecular butt.

The crystal structure of the MMP-9 protein was screened from the protein structure PDB database (**https://www.rcsb.org/**) to determine the receptor for molecular docking, and metal ions in the receptor structure were retained.[59] A suitable molecular butt of pterostilbene to the receptor 6ESM was performed using MOE software for dehydration, structural correction, partial charge calculation, protonation, and energy minimization prior to the formal butt. Subsequently, molecular docking verification of the ligand pterostilbene to the receptor 6ESM was performed using two software programs, MOE and Autodock 4.2.6, respectively.

2.10 Human brain microvascular endothelial cell (hBMEC) culture

hBMECs (purchased from the Cell Center of Peking Union Medical College) were cultured in DMEM:F12 medium (Biological Industries, USA) supplemented with 10% FBS (PAN-Biotech, Germany), 100 U mL^{-1} penicillin and 0.1 mg mL^{-1} streptomycin (Solarbio, Beijing, China). The cell culture conditions were maintained in 95% air and 5% CO_2 under a humidified atmosphere in a 37 °C incubator (Panasonic, Japan).

2.11 Oxygen-glucose deprivation model

An hBMEC model of oxygen-glucose deprivation (OGD) was established after plating for 24 h. Briefly, in the experiment of actin staining and mechanism exploration, the cells were randomly divided into the control, OGD, pterostilbene (7.5, 15, and 30 μM) + OGD and NBP (20 μM) + OGD groups. The cells were randomly allocated into four groups for the validation experiment of the Wnt pathway inhibitors: control group, OGD group, pterostilbene (30 μM) + OGD group, and XAV-939 (1 μM; APExBIO, Houston, USA) + pterostilbene (30 μM) + OGD group. The medium was replaced with Earle's balanced salt solution, and the cells were placed in an anaerobic incubator (COY Laboratory, USA) to deprive of sugar and oxygen for 1 h (see ESI Fig. 4† for the exploration of hypoxia time). At the end of OGD, cells were replaced with a standard medium containing 1% FBS and returned to a normoxic incubator (37 °C, 5% CO_2). The control cells were incubated under normal conditions and were not exposed to OGD. A schematic diagram of the experimental protocols is shown in Fig. 1C.

2.12 MTT assay

hBMECs were seeded in 96-well culture plates at a density of 3000 cells per well. After the cells were exposed to OGD as mentioned above and incubated with pterostilbene/NBP for 12 h, the MTT cell proliferation and cytotoxicity assay kit (Beyotime Biotech, Shanghai, China) was used to evaluate cell viability according to the manufacturer's manual. Briefly, 10 μL of MTT solution was added to a 96-well plate and incubated for 4 h at 37 °C followed by the addition of a formazan solvent for another 3 h of incubation. The absorbance at 570 nm was measured using a microplate reader (Tecan, Switzerland).

$$\text{Relative cell viability } (\%) = (A_{\text{experiment}} - A_{\text{blank}})/(A_{\text{control}} - A_{\text{blank}}) \times 100\%$$

2.13 hBMEC actin staining

hBMECs were seeded in 6-well culture plates at a density of 2×10^5 cells per well. After the exposure to OGD as mentioned above and the incubation with pterostilbene/NBP for 12 h, the cells were fixed in 4% PFA for 10 min at room temperature followed by washing the fixed cells with PBS three times. Actin staining was done using 488 conjugated Phalloidin-ifluor™ (AAT Bioquest, USA) for 20 min at room temperature. Cells were then stained with Hoechst 33258 (Beyotime Biotech, Shanghai, China) for nuclear labelling at 37 °C for 5 min. After staining, laser confocal microscopy (TCS-SP8 STED 3X, Leica, USA) was performed for observation and imaging purposes.

2.14 Western blotting

Brain tissues or hBMECs were lysed in RIPA buffer containing protease inhibitors and phosphatase inhibitors (100 : 1 : 1) (all purchased from Cowin Biotech Co., Ltd, Jiangsu, China) for 40 min on ice and centrifuged at 14 000*g* for 10 min at 4 °C. The protein concentration was determined based on the BCA method using a protein quantitative analysis kit (Cowin Biotech, Jiangsu, China). The proteins were resolved using SDS-polyacrylamide gel electrophoresis and electrotransferred to PVDF membranes. The membranes were blocked in 5% skim milk (BD, USA) for 2 h at room temperature and then incubated overnight at 4 °C with the primary antibodies shown in Table 1. After the membranes were washed, they

Table 1 Primary antibodies used for western blotting

Primary antibody	Source species	Dilution	Company
Phospho-ADF/cofilin (3313)	Rabbit	1 : 1000	Cell Signaling Technology (Beverly, MA, USA)
Total-ADF/cofilin (5175)	Rabbit	1 : 1000	Cell Signaling Technology (Beverly, MA, USA)
Phospho-MLC (3671)	Rabbit	1 : 1000	Cell Signaling Technology (Beverly, MA, USA)
Occludin (91 131)	Rabbit	1 : 1000	Cell Signaling Technology (Beverly, MA, USA)
VE-cadherin (2500)	Rabbit	1 : 1000	Cell Signaling Technology (Beverly, MA, USA)
β-Tubulin (2128)	Rabbit	1 : 1000	Cell Signaling Technology (Beverly, MA, USA)
MMP-9 (ab76003)	Rabbit	1 : 1000	Abcam (Cambridge, UK)
Wnt/beta catenin signaling pathway (ab228526)	Rabbit	Cyclin D1 1 : 10 000; the other – 1 : 1000	Abcam (Cambridge, UK)
ROCK1/2 (ab45171)	Rabbit	1 : 2000	Abcam (Cambridge, UK)
F-actin (ab130935)	Mouse	1 : 500	Abcam (Cambridge, UK)
G-actin (ab200046)	Rabbit	1 : 1000	Abcam (Cambridge, UK)
Claudin-5 (ab131259)	Rabbit	1 : 1000	Abcam (Cambridge, UK)
ZO-1 (21773-1-AP)	Rabbit	1 : 1000	Proteintech (Rosemont, IL, USA)
Laminin (NB300-144SS)	Rabbit	1 : 1000	Novus (Colorado, USA)
β-Actin (abs119600)	Rabbit	1 : 5000	Absin (Shanghai, China)

were incubated with a HRP-conjugated secondary antibody for 2 h at room temperature. The immunoblots were scanned and analyzed using a chemiluminescence imager (Bio-Rad, USA) and quantified using ImageJ software.

2.15 Statistical analysis

Data were presented as the mean ± standard deviation (SD). One-way ANOVA and two-tailed unpaired *T* test were used for comparison between groups, and $P < 0.05$ was considered statistically significant. Statistical analysis was performed with GraphPad Prism software.

3. Results

3.1 Pterostilbene treatment improved neurological dysfunction and increased the survival rate in MCAO rats

The modified neurological severity score (mNSS) was assessed 3, 7, and 14 days after the MCAO surgery, respectively. As shown in Fig. 2A, neurological function was impaired after cerebral I/R injury. Treatment of NBP significantly improved the neurological function 3 days after the MCAO surgery with a 56% reduction in the mNSS score ($P < 0.05$). Treatment of pterostilbene did not show significant improvement. 7 days after surgery, groups with the treatment of NBP and pterostilbene (30 and 60 mg kg^{-1}) showed significantly improved neurological function, with 63%, 38% and 63% reduction in the mNSS score compared with the model group, respectively ($P < 0.05$). At this time, the high-dose pterostilbene group showed comparable effects with the group treated with the positive drug NBP. 14 days after surgery, all drug groups showed significant improvement in neurological function ($P < 0.05$). At this time, the improvement of neurological dysfunction in MCAO rats resulted by high-dose pterostilbene was superior to that of the positive drug NBP, while the medium-dose pterostilbene group was comparable to the NBP group.

For 14 days after surgery, drugs were administered daily, and survival rates were recorded, as shown in Fig. 2B–I. In terms of increasing survival rate, the effects of all treatments were similar in the acute phase (the first 3 days), but in the recovery phase, the efficacy of the pterostilbene groups was better than that of the resveratrol and NBP groups, and showed a good dose dependence.

Taken together, these results suggested that the administration of pterostilbene significantly improved neurological deficits and increased the survival rate of MCAO rats.

3.2 Pterostilbene treatment reduced cerebral infarction volume in MCAO rats

TTC staining showed that the infarction volume of NBP (13.86 ± 7.40%), resveratrol (15.98 ± 4.87%) and high-dose pterostilbene treatments (16.10 ± 10.31%) were reduced compared with the model group (32.15 ± 9.50%) 3 days after cerebral I/R injury (Fig. 3A and B). 7 days after reperfusion, pterostilbene reduced infarction volume in a dose-dependent manner, and the effects of low, medium and high-dose treatments were stronger than those of the positive drugs resveratrol and NBP. Pterostilbene (60 mg kg^{-1}) (7.80 ± 2.92%) had the best effect on reducing the infarction volume, which was only 30% of the infarct volume in the model group (26.19 ± 16.32%) (Fig. 3C and D). 14 days after reperfusion, the cerebral infarction volume in the high-dose pterostilbene treatment group (7.24 ± 4.17%) was significantly reduced compared with the model group (19.08 ± 7.94%), and the effect was stronger than those of the resveratrol and NBP groups (Fig. 3E and F). These results indicated that pterostilbene had a good effect on the reduction of cerebral infarction volume in the subacute and recovery stages.

3.3 Pterostilbene treatment promoted CBF recovery and reduced BBB leakage in MCAO rats

Cerebral microvascular status is closely related to BBB function, and microcirculatory blood flow can serve as a potential demonstration of BBB function. To determine the potential therapeutic benefits of promoting the recovery of cerebral microcirculation, we used a laser speckle imaging technique to

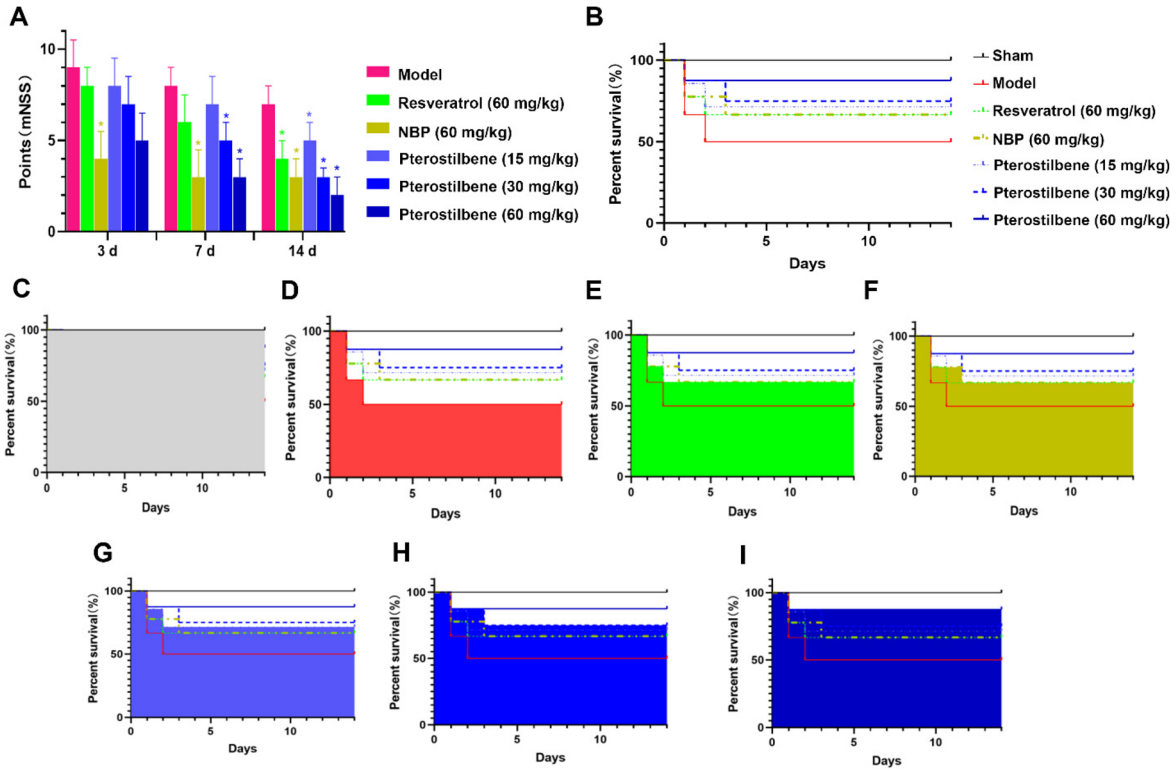

Fig. 2 Pterostilbene and positive drug treatments improved neurological dysfunction and survival rate in MCAO rats. (A) The mNSS scores of MCAO rats 3, 7, 14 days after MCAO surgery in each group. n = 6, mean ± SD.*P < 0.05 *vs.* the model group. (B) Overview of the survival rate of rats in each group that lasted until 14 days. (C–I) The survival rate of rats in each group that lasted until 14 days.

evaluate CBF changes during ischemia and reperfusion (Fig. 4A and B). After cerebral I/R injury, the CBF of the ischemic side decreased to 60%, indicating successful modeling. 3 days after reperfusion, NBP treatment (86.87 ± 3.33% of the baseline) led to better recovery of CBF than the model group (69.43 ± 14.47% of the baseline), showing an advantage in the recovery of CBF in the acute phase. In contrast, the recovery of CBF in the other treatment groups was better than that in the model group, but there was no significant difference. 7 days after reperfusion, the high-dose pterostilbene treatment (90.62 ± 10.55% of the baseline) and resveratrol treatment (92.36% ± 6.94% of the baseline) basically recovered to the level of NBP (94.15 ± 10.80% of the baseline) compared with the model group (68.52 ± 5.02% of the baseline). 14 days after reperfusion, the high-dose pterostilbene treatment and resveratrol treatment still maintained the same recovery effect as NBP, while the medium-dose pterostilbene and low-dose pterostilbene treatments also resulted in some recovery, showing a certain level of dose dependence. These results indicated that the pterostilbene treatment promoted the recovery of CBF on the ischemic side mainly in the subacute and recovery phases of cerebral I/R rats, showing good time-dependence and dose-dependence.

To assess the permeability of the BBB, EB leakage was measured 1 day after reperfusion. Representative images of the EB dye in the brain tissue, as shown in Fig. 5A, showed significant EB extravasation in the ischemic hemisphere of the model group, and extravasation was slightly reduced in each treatment group (with pterostilbene selected at the high dose of 60 mg kg^{-1} in the treatment group). Quantitative results showed that the content of EB in the pterostilbene treatment group (0.97 ± 0.16 μg g^{-1} pro) was significantly lower than that in the model group (4.23 ± 0.33 μg g^{-1} pro), and was similar to that in the positive drug NBP (1.17 ± 0.35 μg g^{-1} pro) and resveratrol (1.99 ± 0.55 μg g^{-1} pro) treatment groups (Fig. 5B). The results showed that pterostilbene had a good protective effect on the BBB in the early stage.

To further investigate the impact of pterostilbene on the BBB structure, we evaluated the expression of intercellular junctions and the extracellular matrix following treatment with pterostilbene (60 mg kg^{-1}). The representative western blot images of the ischemic brain tissue are presented in Fig. 5C. After I/R injury, the expressions of junctional (ZO-1, occludin, claudin-5 and VE-cadherin) and basal membrane (BM-laminin) proteins were significantly reduced, while that of pterostilbene was increased after the treatment, indicating its contribution to the restoration of the BBB. The quantitative results at each time point shown in Fig. 5D revealed that pterostilbene significantly enhanced the expressions of BBB structural proteins during the acute (1 day), subacute (3 days) and recovery stages (7 and 14 days) following I/R injury, with particularly notable effects observed during the recovery stage.

The above results indicated that pterostilbene significantly restored cerebral microcirculatory blood flow, improved BBB per-

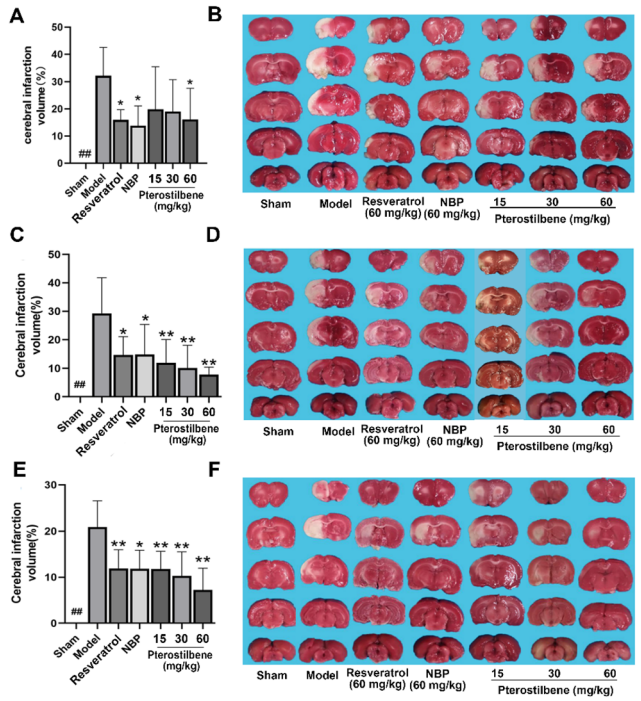

Fig. 3 Pterostilbene and positive drug treatments reduced cerebral infarction volume in MCAO rats. (A, C and E) The percentage of cerebral infarction volume at 3, 7, and 14 days after reperfusion. (B, D and F) Representative images of brain slices stained with TTC at 3, 7, and 14 days after the reperfusion. n = 6, mean ± SD. *P < 0.05 and **P < 0.01 *vs.* the model group.

meability and increased the expression of structure-related proteins, thereby providing further protection to the BBB and promoting its function. Additionally, the protective effect of pterostilbene on the BBB was observed throughout all phases after I/R injury, including the acute, subacute and recovery phases, with the most significant effect during the recovery phase.

3.4 Pterostilbene may target MMP-9 for the therapeutic effects on stroke

A total of 10 stroke-related targets were identified using the Thomson Reuters Integrity and TTD databases and literature analysis,[51] namely, F3, F10, F11, MMP-9, P2RY1, TBXA2R, VEGFA, SERPINE1, THBD, and P2RY12. Four coagulation system-related targets, three platelet-related targets, two vascular endothelial protection targets, one fibrinolytic system target, the specific names, UniProt serial numbers and functions are shown in Table 2.

3.5 Pterostilbene bound to MMP-9 and had strong binding activity

Molecular docking analysis was applied to confirm whether pterostilbene binds to the MMP-9 proteins. The docking score was used as a criterion for judging the ligand–receptor binding activity, with some binding activity when the docking score was less than −4.25 kcal mol^{-1}, good binding activity when it was less than −5.50 kcal mol^{-1}, and strong binding activity when it was less than −8.00 kcal mol^{-1}. The docking score of −7.35 kcal mol^{-1} for MOE and −8.53 kcal mol^{-1} for AutoDock 4.2.6 both indicate that pterostilbene can interact with the receptor 6ESM directly with strong binding activity. ALA-189 was the key amino acid residue of 6ESM (Fig. 6). The findings further indicated that pterostilbene exhibits a strong binding activity towards MMP-9, which may be attributed to the amino acid residue ALA-189.

3.6 Pterostilbene treatment alleviated glucose deficiency and hypoxic injury on hBMECs and repaired the morphology of actin

The efficacy results of pterostilbene were further validated by inducing OGD injury of hBMECs *in vitro*. After OGD injury, hBMECs obviously shrunk and rounded, and the adherence was weakened, accompanied by the loss of cell viability (P < 0.05). Pterostilbene incubation (12 h) inhibited the loss of cell viability caused by OGD injury in a concentration-dependent manner, showing a protective effect against glucose deficiency and hypoxic injury *in vitro* (Fig. 7A).

Actin staining was performed to visualize the changes in the actin structure. 3 h and 12 h after OGD injury, actin showed a blurred morphology and decreased density, while pterostilbene repaired the damage of actin morphology (Fig. 7B–M). Quantitative analysis of the fluorescence intensity showed that the repair effect of pterostilbene was significantly

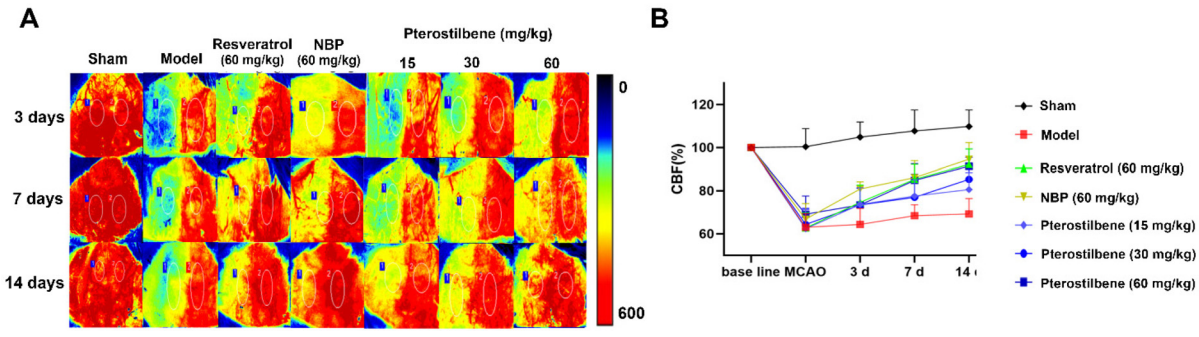

Fig. 4 Pterostilbene and positive drug treatments promoted CBF recovery in MCAO rats. (A) Representative images of CBF in each group at 3, 7, and 14 days after reperfusion. (B) CBF was quantified and expressed as percentage change from the baseline.

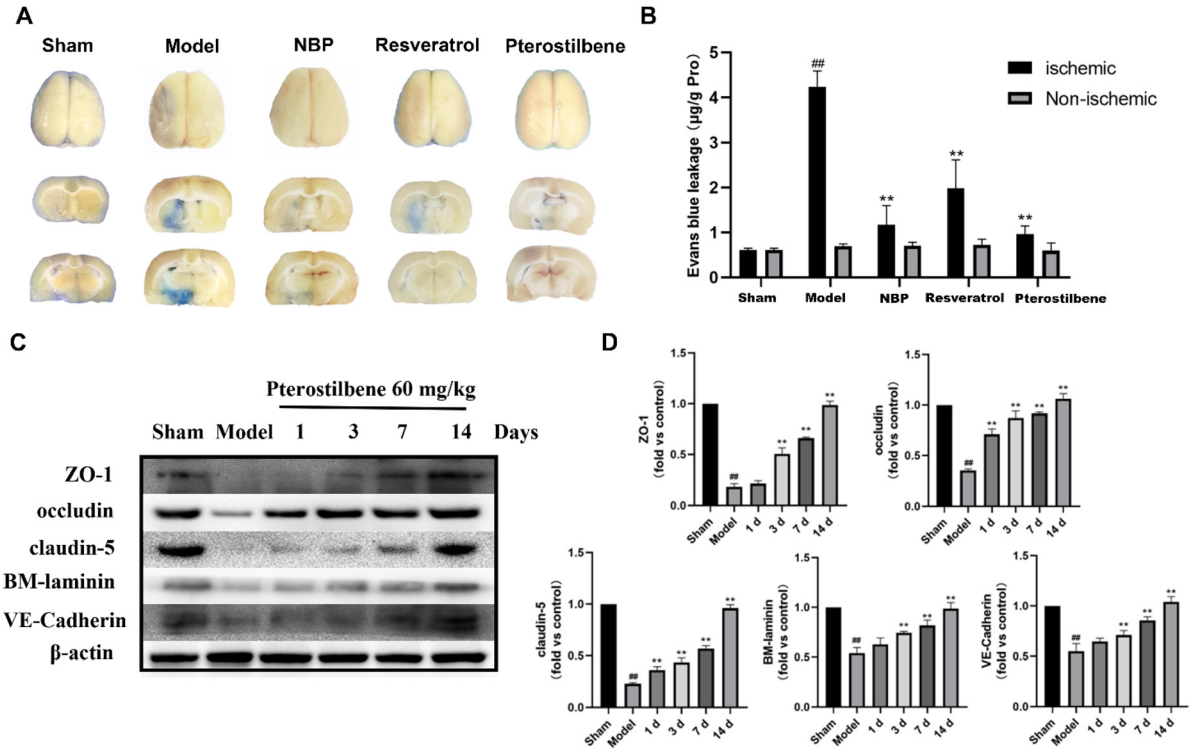

Fig. 5 Pterostilbene treatment reduced BBB leakage and enhanced the expression of junction proteins in MCAO rats. (A) Representative images of rat brain slices in each group. (B) EB leakage rate of rats in each group. n = 6, mean ± SD. $^{**}P < 0.01$ *vs.* the model group. $^{\#\#}P < 0.01$ *vs.* the model group. (C) Representative western blot images showing ZO-1, occludin, claudin-5, BM-laminin and VE-cadherin expressions in the ischemic rat brain tissue. (D) Effects of pterostilbene on improving the expression of intercellular junctions and the extracellular matrix. $n \geq 3$, mean ± SD. $^{\#\#}P < 0.01$ *vs.* the control group. $^{**}P < 0.01$ *vs.* the model group.

Table 2 Names and classification of stroke-related targets

Target symbol	Target name	UniProt accession number	Function
Tissue factor	F3	P13726	Coagulation system
Coagulation factor X	F10	P00742	Coagulation system
Coagulation factor XI	F11	P03951	Coagulation system
Matrix metalloproteinase-9	MMP9	P14780	Vascular endothelium
P2Y purinoceptor 1	P2RY1	P47900	Platelet-related target
Thromboxane A2 receptor	TBXA2R	P21731	Platelet-related target
Vascular endothelial growth factor A	VEGFA	P15692	Vascular endothelium
Plasminogen activator inhibitor I	SERPINEI	P05121	Fibrinolytic system
Thrombomodulin	THBD	P07204	Coagulation system
P2Y purinoceptor 12	P2RY 12	Q9H244	Platelet-related target

Based on the established machine learning model, reverse targeting was used to predict the potential target of pterostilbene for stroke treatment. The only positive "TRUE" result obtained was for MMP-9, indicating that pterostilbene may act on this target.

dose-dependent and stronger than that of positive drug NBP (Table 3).

3.7 Pterostilbene inhibited OGD-induced early stress fiber formation and junction protein reorganization by overexpressing ADF

Stress fibers are contractile bundles of cross-linked F-actin formed by stress-induced actin polymerization, generating tension against cell–cell and cell–matrix junctions and increasing endothelial paracellular permeability.[60] Our results demonstrated that pterostilbene had a significant distribution on the cytoskeleton of hBMECs (see ESI Fig. 5B†). To investigate the protective effect of pterostilbene on the cytoskeleton and the underlying mechanisms, we evaluated the formation of stress fibers in the cytoskeleton induced by OGD and the expression of corresponding proteins in its regulatory pathways by western blot analysis. OGD-induced hBMEC actin cytoskeletal rearrangement occurred by promoting the formation of F-actin from G-actin, a sign of stress fiber formation (Fig. 8A). The ratio of F/G-actin in hBMECs increased signifi-

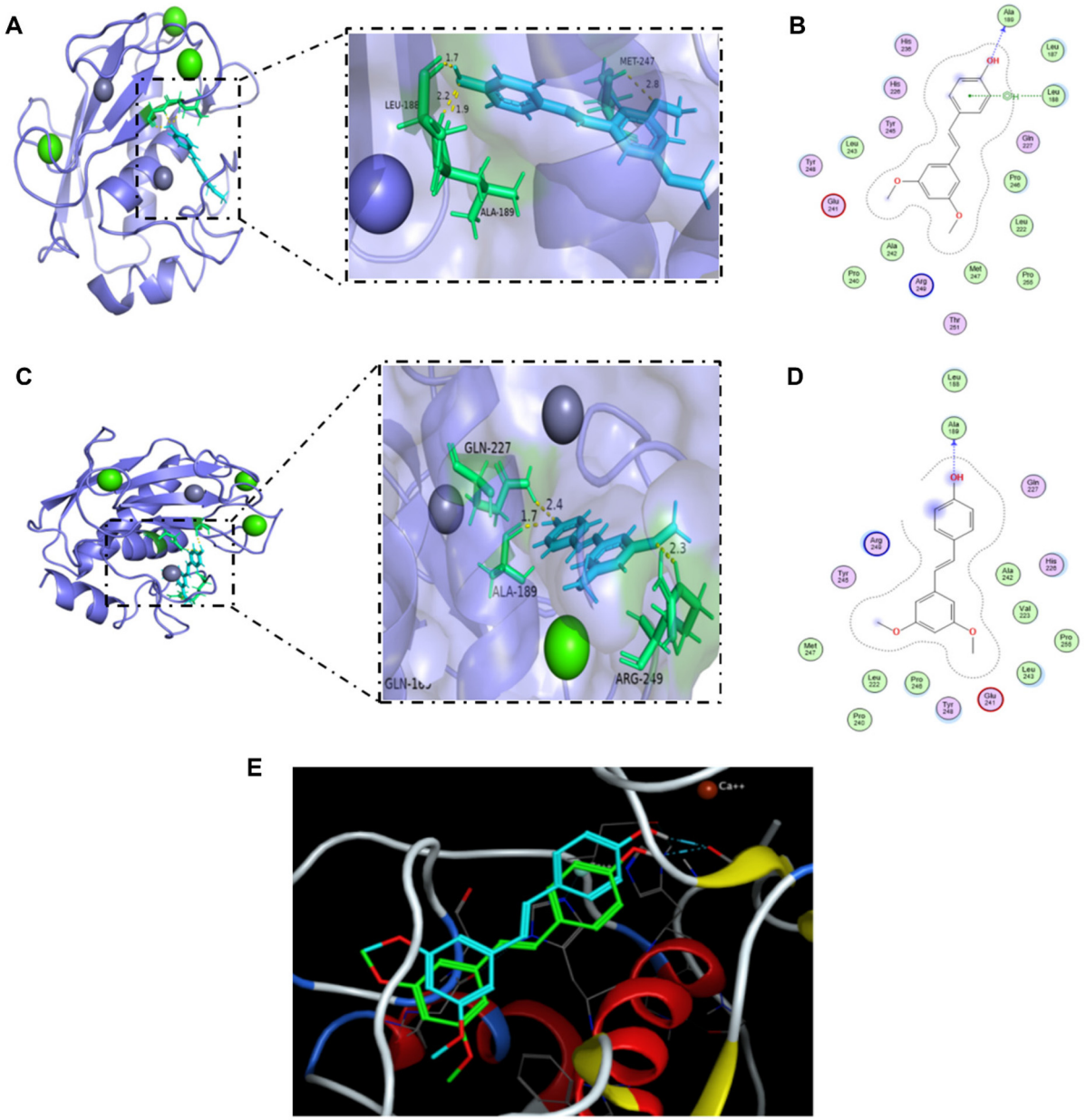

Fig. 6 Molecular docking of the ligand pterostilbene to the receptor 6ESM. (A) 3D interaction diagram of the MOE docking results. The ligand structure is shown in blue, and the nearby residues are shown in green. The skeleton of the receptor is shown in light purple. (B) 2D interaction diagram of the MOE docking results. (C) 3D interaction diagram of the AutoDock 4.2.6 docking results. The ligand structure is shown in blue, and the nearby residues are shown in green. The skeleton of the receptor is shown in light purple. (D) 2D interaction diagram of the AutoDock 4.2.6 docking results. (E) Comparison of the docking results between MOE software and AutoDock 4.2.6 software. The ligand structure in blue is the docking result of the MOE software, and the ligand structure in green is the result of AutoDock 4.2.6.

cantly as early as 3 h after OGD (0.44 ± 0.04 *vs.* the control (0.19 ± 0.02), $P < 0.01$), while pterostilbene dose-dependently inhibited the formation of stress fibers (0.37 ± 0.07; 0.030 ± 0.07; 0.23 ± 0.07, $P < 0.01$) (Fig. 8B and C).

Phosphorylation of myosin light chain (MLC) promotes the formation of dense stress fibers from short F-actins, whereas Rho-associated protein kinase (ROCK) enhances MLC phosphorylation by inhibiting MLC phosphatase activity. As verified by the western blot analysis, there were no significant differences in ROCK and pMLC proteins between the OGD group and the treated group (Fig. 8D), so it was judged that pterostilbene may not regulate stress fiber formation through this pathway.

The actin depolymerization factor (ADF)/cofilin family regulated the balance between actin filament assembly and disassembly, and was active upon dephosphorylation and caused actin depolymerization. To further confirm the pathway by which pterostilbene inhibited stress fiber formation, the

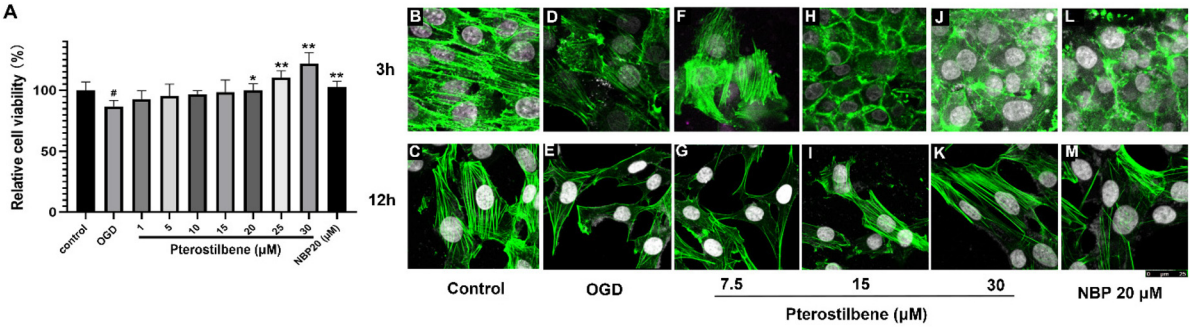

Fig. 7 Pterostilbene treatment inhibited the loss of hBMEC viability and protected actin after OGD injury. (A) Effects of different concentrations of pterostilbene (1–30 μM) on cell viability after OGD injury. n = 3, mean ± SD. $^{\#\#}P < 0.01$ *vs.* the control group, $^{*}P < 0.05$ and $^{**}P < 0.01$ *vs.* the OGD group. (B–M) Confocal fluorescence microscopy images of actin morphology (shown in green) in hBMECs under OGD injury and after drug administration. The scale bar represents 25 μm.

Table 3 Fluorescence intensity analysis of actin staining

	Control	OGD	Pterostilbene 7.5 μM	Pterostilbene 15 μM	Pterostilbene 30 μM	NBP 20 μM
3 h	100.00%	56.30%$^{\#\#}$	81.85%**	87.22%**	94.04%**	88.38%**
12 h	100.00%	50.10%$^{\#\#}$	54.00%	60.39%**	81.87%**	52.97%

$^{\#\#}P < 0.01$ *vs.* the control group, $^{**}P < 0.01$ *vs.* the OGD group.

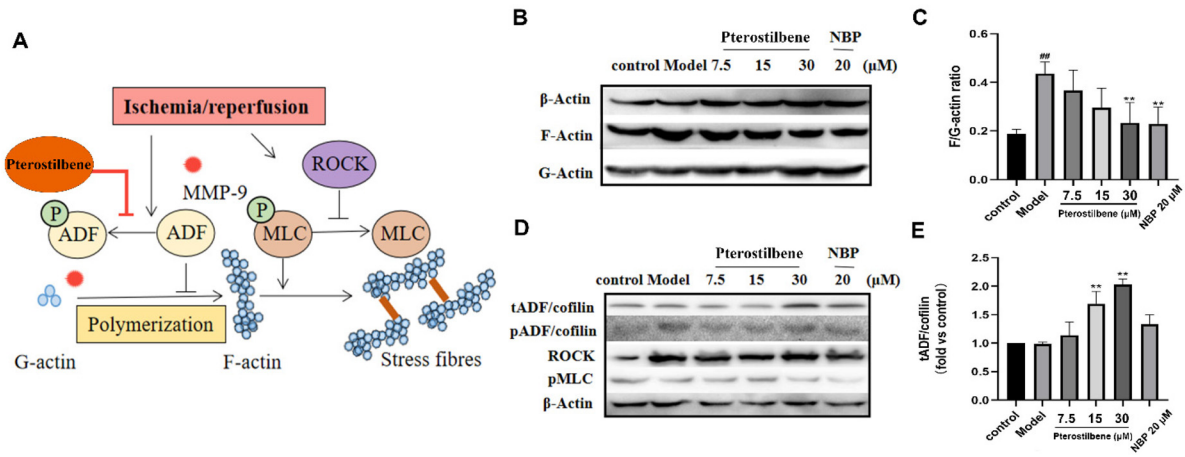

Fig. 8 Pterostilbene inhibited OGD-induced early stress fiber formation. (A) Schematic diagram of the pathway to regulate stress fibers. (B) Representative western blot images showing β-actin, F-actin and G-actin expressions. (C) Pterostilbene decreased the F/G-actin value. (D) Representative western blot images showing tADF, pADF, ROCK and pMLC expressions. (E) Pterostilbene increased the tADF/cofilin expression. $n \geq 3$, mean ± SD. $^{\#\#}P < 0.01$ *vs.* the control group. $^{**}P < 0.01$ *vs.* the model group.

expressions of phosphorylation of ADF/cofilin (pADF/cofilin) and total ADF/cofilin (tADF/cofilin) were analyzed. The expression of pADF was significantly higher in the OGD group than in the control group, indicating that oxygen-glucose deprivation promoted stress fiber formation, while there was no significant change in the other treatment groups. Pterostilbene increased the expression of tADF in a dose-dependent manner (1.14 ± 0.19; 1.69 ± 0.18; 2.03 ± 0.07, $P <$ 0.01), while pADF showed no change, indicating that pterostilbene inhibited actin polymerization to stress fibers by increasing the expression of non-phosphorylated ADF (Fig. 8D and E). ADF overexpression of pterostilbene blocked the deterioration of BBB disruption by targeting early cytoskeletal structural changes in hBMECs. Sustained ADF activity provides long-term improvement in function by reducing early BBB damage and subsequent tissue damage through overexpression of non-phosphorylated ADF.

In endothelial cells, early actin polymerization and stress fiber formation lead to cell contraction and redistribution/disassembly of junction proteins (JPs). We further verified the

effect of pterostilbene treatment on JP rearrangement using western blotting. 3 h after OGD, the distribution of occludin, claudin-5, and VE-cadherin shifted from the membrane fraction to the actin cytoskeleton fraction (ACF) at the hBMEC extracellular cell–cell contact site (Fig. 9B–E), whereas their total expression in whole cell lysates remained unchanged. After pterostilbene incubation, the redistribution of JPs was significantly inhibited.

The redistribution of occludin, claudin-5 and VE-cadherin may be related to the tension generated by stress fibers and cell contraction. Together, these results suggested that OGD-induced hBMEC structural changes, including actin polymerization and JP redistribution, occurred at an early phase after I/R, and led to BBB disruption. Pterostilbene had a good inhibitory effect on the above two aspects by overexpressing ADF, so as to improve the early BBB destruction and lay the foundation for long-term BBB protection.

3.8 Pterostilbene inhibited OGD-induced BBB damage by regulating the Wnt pathway and MMP-9 expression

MMP-9 is an enzyme that degrades the main components of BM during cerebral I/R. Its degradation of JPs and BM occurs after structural changes of the endothelial cytoskeleton. Based on the above results, our western blot analysis confirmed that pterostilbene increased the expression of the TJ key proteins ZO-1, occludin, and claudin-5, the AJ key protein VE-cadherin and the basement membrane component BM-laminin after OGD injury (12 h) (Fig. 10A–F). At the same time, pterostilbene reduced the expression of MMP-9 induced by OGD, and the effect was better than that of NBP. MMP-9 is a direct transcriptional target of the Wnt/β-catenin signaling pathway. Continuous activation of the Wnt signaling pathway can reduce the expression of MMP-9 and repair BBB damage. Pterostilbene upregulated the expressions of c-Met, c-Jun and c-Myc proteins in the Wnt pathway in a dose-dependent manner (Fig. 10G–K), and showed its protective effect on the BBB.

To further validate the role of pterostilbene in the Wnt pathway, we added a Wnt pathway inhibitor XAV-939 (1 μM) to investigate the expression of key proteins in the Wnt pathway and BBB junction. As depicted in Fig. 11, XAV-939 significantly suppressed pterostilbene-induced upregulation of junction proteins after 12 h of OGD/R. Moreover, pterostilbene's inhibitory effect on MMP-9 production and the activation of key proteins in the Wnt pathway was also markedly attenuated.

These findings demonstrate that pterostilbene modulated the expression of MMP-9 and key BBB junction proteins *via* the Wnt pathway during the late stage of ischemia-reperfusion injury.

4. Discussion

In the present study, pterostilbene had a good therapeutic effect on cerebral I/R injury, embodied in the following aspects: pterostilbene markedly improved neurological function, increased the survival rate, decreased the cerebral infarction volume and promoted weight gain (see ESI Fig. 1†). In addition, pterostilbene improved the recovery of cerebral microcirculation and reduced BBB leakage, promoting the function and structural integrity of the BBB. We also demonstrated that pterostilbene protected hBMECs from OGD-induced cell viability loss and actin damage *in vitro*, indicating that the anti-cerebral I/R effect of pterostilbene may be exerted by protecting BMECs, the major component of the BBB. It was

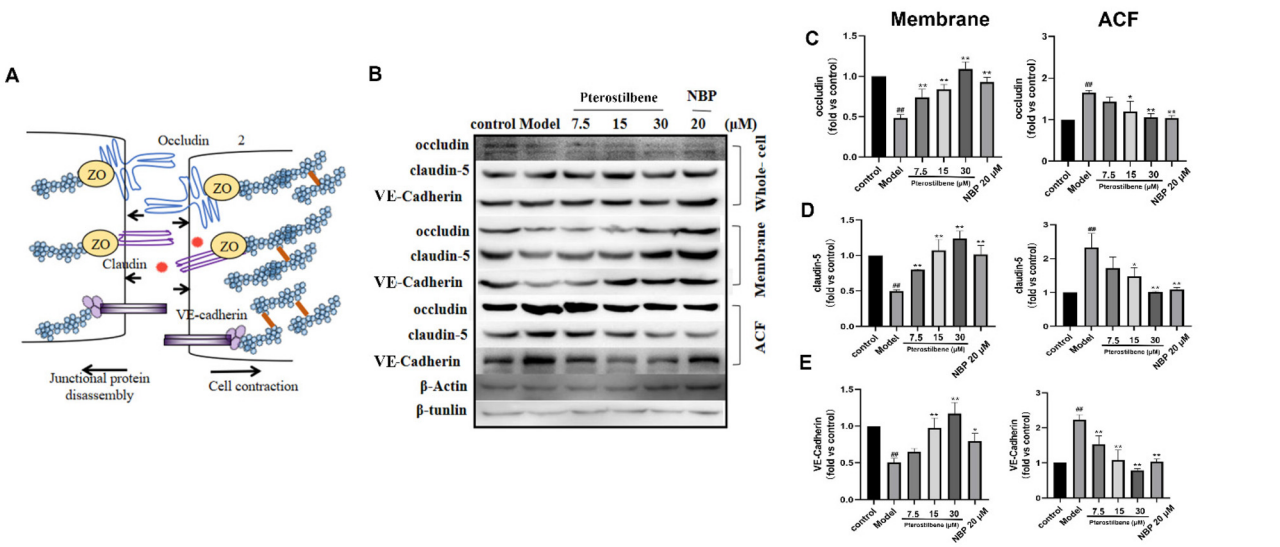

Fig. 9 Pterostilbene inhibited junction protein redistribution. (A) Schematic diagram of the JPs of the BBB. (B) Representative western blot images showing occludin, claudin-5 and VE-cadherin expressions. (C–E) Effects of pterostilbene on occludin, claudin-5 and VE-cadherin protein expressions of total, membrane, and actin cytoskeleton fraction (ADF) proteins of hBMECs after OGD 3 h. $n \geq 3$, mean ± SD. $^{\#}P < 0.05$ and $^{\#\#}P < 0.01$ *vs.* the control group. $^{*}P < 0.05$ and $^{**}P < 0.01$ *vs.* the model group.

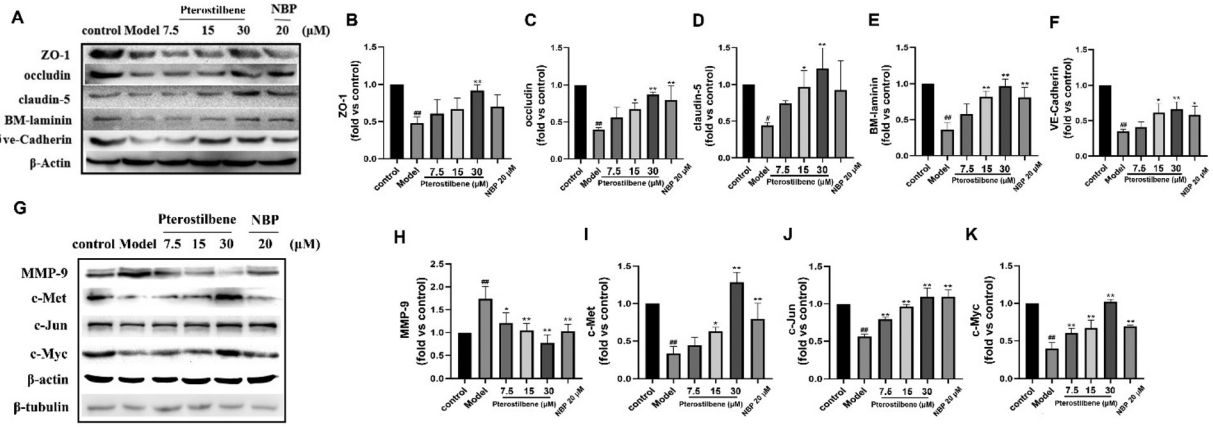

Fig. 10 Pterostilbene inhibited BBB damage. (A) Representative western blot images showing ZO-1, occludin, claudin-5, BM-laminin and VE-cadherin expressions. (B–F) Effects of pterostilbene on TJ (ZO-1, occludin and claudin-5), BM component (BM-laminin) and AJ (VE-cadherin) protein expressions of hBMECs after OGD 12 h. (G) Representative western blot images showing MMP-9, c-Met, c-Jun and c-Myc expressions. (H–K) Effects of pterostilbene on MMP-9 and the key proteins in the Wnt signaling of hBMECs after OGD 12 h. $n \geq 3$, mean ± SD. $^{\#}P < 0.05$ and $^{\#\#}P < 0.01$ *vs.* the control group. $^{*}P < 0.05$ and $^{**}P < 0.01$ *vs.* the model group.

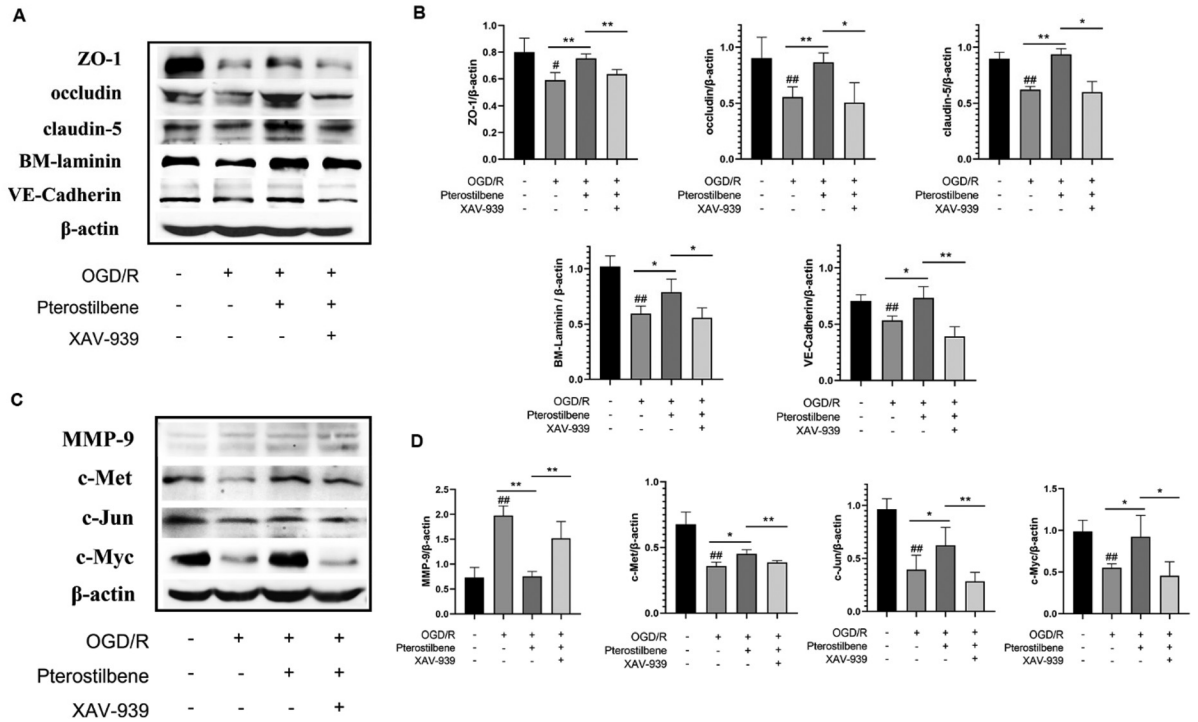

Fig. 11 XAV-939 effectively attenuated the regulatory impact of pterostilbene on MMP-9 expression, Wnt pathway proteins and junction proteins. (A) Representative western blot images showing ZO-1, occludin, claudin-5, BM-laminin and VE-cadherin expressions. (B) Effects of pterostilbene and XAV-939 on TJ (ZO-1, occludin and claudin-5), BM component (BM-laminin) and AJ (VE-cadherin) protein expression of hBMECs after OGD 12 h. (C) Representative western blot images showing MMP-9, c-Met, c-Jun and c-Myc expressions. (D) Effects of pterostilbene and XAV-939 on MMP-9 and the key proteins in the Wnt signaling of hBMECs after OGD 12 h. $n \geq 3$, mean ± SD. $^{\#}P < 0.05$ and $^{\#\#}P < 0.01$ *vs.* the control group. $^{*}P < 0.05$ and $^{**}P < 0.01$ *vs.* the corresponding group.

further confirmed that pterostilbene protected against OGD-induced BBB injury by targeting early endothelial structural changes, such as stress fiber formation and JP rearrangement, and then inhibited the degradation of BM components by inhibiting the activity of MMP-9 through the Wnt signaling pathway. The dual action stages jointly protected the BBB, and promoted long-term functional improvement after cerebral I/R (Fig. 12). This is the first study to reveal that pterostilbene has a protective effect against BBB injury during ischemic stroke, and its protective mechanism has been elucidated. Our results

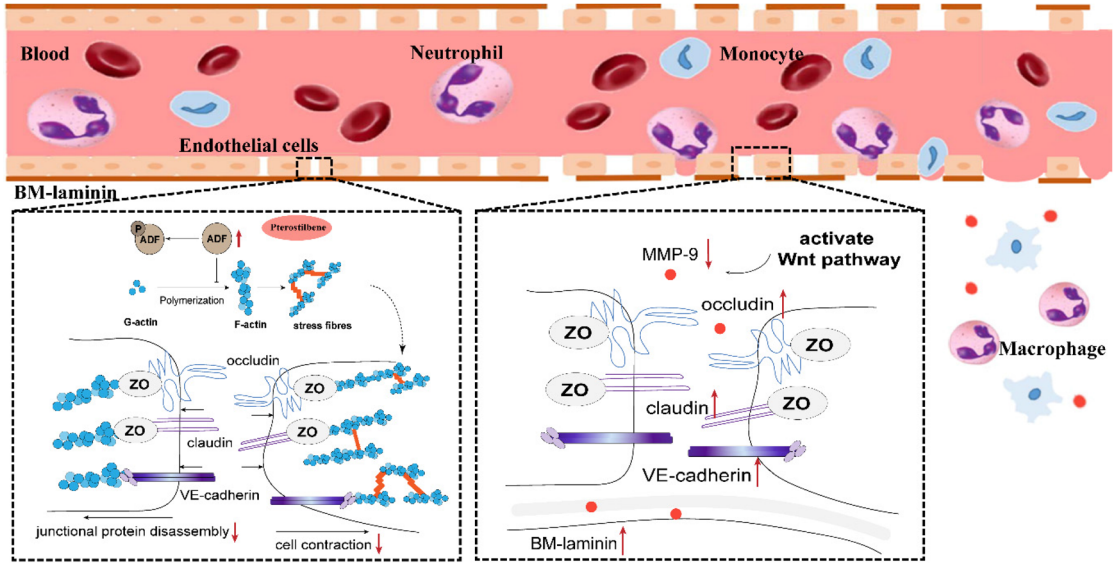

Fig. 12 Improved effect of pterostilbene on the underlying mechanism of BBB disruption following stroke.

suggest that protection of BMECs, the main components of the BBB, is of great significance for the subsequent treatment of ischemic stroke and provide a theoretical basis for the treatment of ischemic cerebrovascular diseases.

4.1 Evaluation of the anti-cerebral ischemia effect of pterostilbene

In this study, we used a classical rat MCAO model to evaluate the cerebrovascular protective effect of pterostilbene. Since MCA and its branches are most commonly affected by stroke,[61] MCAO models have been widely used in the field of preclinical stroke. Rat cerebral arteries are highly similar to those of humans in terms of structural and morphological changes in the vessel wall related to cerebrovascular diseases[62] and are widely used (approximately 66% of *in vivo* models[63]). Therefore, the rat MCAO model is one of the closest models to human ischemic stroke[64] and is highly justified for pharmacodynamic validation of ischemic stroke. The occlusion of MCA blood flow causes focal blood supply disorder of the brain tissue, resulting in hypoxic–ischemic lesions, forming cerebral infarction areas, and further causing neurological deficits. Cerebral microvasculature makes up 85% of the vasculature of the brain and is the principal contributor to BBB function.[65] Therefore, changes in cerebral microcirculation can also be a key indicator to evaluate BBB function. After cerebral I/R injury, restoring microcirculation reperfusion is essential to rescue the penumbra, which is conducive to the overall recovery of ischemia. Our results demonstrated that pterostilbene had a prominent effect on the recovery of neurological function, the reduction of cerebral infarction volume and the restoration of microcirculation blood flow, and resulted in a significant improvement in the survival rate of the experimental rats. In the process of cerebral I/R, oxidative stress, inflammation and BBB dysfunction begin to occur a few hours after ischemia,[6] which will cause many adverse secondary injuries. According to our results, pterostilbene had a good effect on the recovery of cerebral microcirculation and reduction of BBB leakage and structural damage, indicating the potential role in the regulation of BBB function and structure. In this process, we also observed that NBP, as a drug used in the clinical acute phase of cerebral ischemia, had the best effect on the reduction of cerebral infarction volume, the recovery of cerebral circulation and the improvement of neurological function after 3 days of administration, which was consistent with its application scope.[20] Pterostilbene is superior to or equivalent to NBP in the subacute and recovery phases. In the acute phase, pterostilbene is inferior to NBP, but still has significant effects. Pterostilbene was more effective than NBP and resveratrol in reducing EB leakage in the acute phase due to its higher lipid solubility, which allowed pterostilbene to easily penetrate the BBB. Such results give us a reasonable prediction that pterostilbene combined with the positive drug NBP can be used simultaneously in the acute, subacute and recovery phases of cerebral ischemia and cover all pathological process after cerebral I/R.

Under physiological conditions, the BBB is a dynamic exchange interface with selective permeability between blood and brain parenchyma, which strictly controls the entry of harmful substances. During and after cerebral ischemia, high permeability caused by the structural changes of the BBB can cause disabling of sequelae, such as vasogenic edema and HT and inflammatory reactions, causing incalculable secondary damage.[66] Endothelial cells are the central units and the basic structures of the BBB,[67] which are important for maintaining the integrity of the BBB. Their dysfunction is a sign of ischemic cerebrovascular disease,[68] and may also aggravate the disease of acute ischemic stroke and affect the ultimate degree of tissue damage. In this study, hBMECs were used to investi-

gate the ability of pterostilbene to protect against OGD injury *in vitro*. The results showed that when induced by appropriate hypoxia time (see ESI Fig. 3†), pterostilbene (20–30 μM) effectively promoted the survival of hBMECs and reversed the loss of cell viability. At the same time, we also found that pterostilbene was able to promote the repair of actin in hBMECs to maintain better support. These results laid a foundation for the subsequent study of the mechanism of endothelial cell protection.

4.2 Prediction of the potential target for the anti-cerebral ischemia effect of pterostilbene

In this study, we utilized two computer-aided tools to validate each other, machine learning model starting with the stroke disease and the available active drugs, and molecular docking starting with the molecular structure of the compound. After deducing the binding receptor MMP-9, we performed the same pattern of molecular docking for resveratrol and pterostilbene, respectively. The semi-flexible docking of resveratrol to the MMP-9 receptor yielded a docking score of −6.69 kcal mol^{-1} (see ESI Fig. 2†), exhibiting a good binding activity. As a structural analogue of resveratrol, pterostilbene exhibited superior binding ability to MMP-9 with a docking score of −7.35 kcal mol^{-1}. This binding difference may be closely related to the structure of the compound. The two substituted methoxy groups of pterostilbene may have an enhanced effect on the binding ability of the compound to the receptor compared to the three phenolic hydroxyl substitutions of resveratrol. This inference may contribute to the structural modification of active compounds, but further experimental confirmation is needed.

MMP-9, as the major matrix metalloproteinase, directly degrades the basement membrane and other components of the BBB after cerebral ischemia and is closely associated with the destruction of the BBB. Guo *et al.*[69] used a combination of immunohistochemistry and gelatin zymography to demonstrate that MMP-9 positive cells were present in large numbers in the brain tissue of rats in the MCAO group, and that MMP-9 activity was significantly enhanced. Liu *et al.*[70] also found a significant increase in MMP-9 expression in the cortex and striatum of the rat brain tissue in the MCAO group. Such results were consistent with the changes in BBB permeability and brain water content. In recent studies, MMP-9 activation induced by delayed t-PA treatment is a key factor in causing BBB injury and HT in stroke models.[71] All of the above recent findings can confirm that BBB injury during cerebral ischemia is closely related to MMP-9. In order to reduce the damage of the BBB during cerebral ischemia and avoid more serious secondary damage, drug therapy may also focus on this target for inhibition and treatment.

4.3 Possible mechanisms for pterostilbene treatment to improve BBB disruption after I/R injury

Matrix metalloproteinases (MMPs) are a group of zinc-dependent enzymes that degrade ECM components in the basement membrane, of which MMP-9 is thought to be responsible for cerebral I/R-induced BBB breakdown.[62] Studies have shown that early structural changes in endothelial cells can damage the BBB before the onset of junctional and ECM degradation by MMP-9.[72] Early BBB dysfunction leads to the following progression of subsequent injuries: hypoxia induces the formation of stress fibers in endothelial cells, which is also a sign of endothelial cytoskeletal rearrangement under pathological conditions.[73] Stress fiber contraction anchors the generated tension to the cellular junctions of the actin cytoskeleton and disassembles JPs,[74] facilitating their internalization,[75] and thus destabilizing intercellular junctions and BBB permeability. This disassembly and rearrangement may make ECM more accessible and degradable by MMP-9. At the same time, the accompanied widening of junctions between endothelial cells largely promotes the entry of substances in the blood and the infiltration of circulating immune cells, which leads to secondary tissue damage.

Under physiological conditions, the balance between actin polymerization and depolymerization is precisely regulated. Actin forms adhesion complexes with cell–cell or cell–matrix and maintains paracellular permeability by regulating the dynamic balance between them.[76] When actin is disrupted, it leads to imbalance and high permeability of the BBB. BMECs are constantly subjected to mechanical stress at the interface with blood by hydrostatic pressure and fluid shear, which stimulate stress fiber formation when the pressure is excessive.[72] The ADF/cofilin family, ROCK and MLC are three crucial pathways involved in regulating actin polymerization and stress fiber formation.[77,78] After I/R, ADF/cofilin is phosphorylated and rapidly inactivated, leading to stress fiber formation and barrier destruction. The activation of ROCK and MLC allows actin in BMECs to interact with the non-muscle myosin to form stress fibers, causing contraction of the cytoskeleton, which leads to BBB disruption during the early stage of cerebral I/R.[18] Both providing sustained ADF activity and inhibiting ROCK/MLC signaling could halt the progression of injury, thereby providing long-term protection against BBB disruption and neurological deficits. In our study, pterostilbene inhibited F-actin polymerization but not ROCK/MLC signaling through ADF overexpression, suggesting that pterostilbene protects the BBB by providing sustained ADF activity to inhibit stress fiber formation. This was accompanied by a reduction in the disassembly and redistribution of JPs in BMECs. After the exposure to OGD-induced injury, TJs and AJs were distributed from the membrane to the actin cytoskeleton, and this outcome was improved by pterostilbene incubation. Thus, pterostilbene plays an important role in the maintenance of the structural integrity of the BBB by providing sustained ADF activity, while inhibiting stress fiber formation and also reducing subsequent JP disassembly and redistribution. Studies of NBP, the acute ischemic stroke therapeutic drug, have shown that its action in the acute phase is related to anti-inflammatory, antioxidant, and anti-apoptotic mechanisms.[79–81] Our study showed that NBP had an effect on the regulation of the endothelial cytoskeleton, but the effect was not as effective as that of pterostilbene, showing the difference between the two drugs in the treatment of the acute phase mechanism.

Molecular docking verified that resveratrol and pterostilbene could bind to the MMP-9 receptor and exert their biological activities. Pterostilbene was found to down-regulate MMP-9 transcription in studies, which was a part of its anticancer activity against breast cancer cells (MCF-7) and prostate cancer cells (PC3).[82] Disruption of BM by hypoxia occurs after structural changes in endothelial cells. As a direct transcriptional target of the Wnt/β-catenin signaling pathway, MMP-9 is a major protein that maintains the integrity and permeability of BBB tight junctions.[13] Continuous activation of the classical Wnt/β-catenin pathway in endothelial cells can decrease MMP-9 expression and restore the damaged BBB under pathological conditions.[83] Ji *et al.* evaluated the protective effect of lithium on the BBB of adult MCAO mice and found that lithium increased the activity of the Wnt/β-catenin signaling pathway in endothelial cells, increased claudin-5 and ZO-1 protein levels, and decreased MMP-9 expression.[84] *In vitro*, Yu *et al.* established the OGD model of the mouse brain microvascular endothelial cell line bEnd.3 and concluded that oxymatrine could reduce BBB damage caused by I/R, and this neuroprotective effect was at least partially dependent on the protein expression levels of CAV1 and MMP-9.[85] In our study, during the late phase after hypoxic injury, pterostilbene activated key proteins in Wnt signaling and promoted the recovery of TJs, AJs and the BM component in hBMECs, improving the integrity of the BBB. In contrast, NBP was less protective against the key proteins of the BBB than pterostilbene, showing differences in the mechanism of action. The results and comparison of the above mechanisms also provide experimental basis for the further combination of the two drugs with different mechanisms to protect ischemic brain tissue.

In previous studies, the research on stroke focused on neurons and brain parenchyma, whereas the direct protection of the BBB has received little attention. However, the use of tPA thrombolytic therapy in the clinic is severely limited because of the risk of hemorrhage transformation when used beyond the therapeutic time window. This also suggests that stroke research in the future must focus on the BBB to improve the safety and efficacy of tPA treatment. In addition, a long-term response to cerebral I/R should also be emphasized to extend the time window for potential treatments.[86]

5. Conclusions

In conclusion, our present study revealed that pterostilbene has an *in vivo* effect of attenuating cerebral I/R injury, and an *in vitro* effect on anti-hypoglycemic hypoxic injury and protecting actin by reducing stress fiber formation and JP redistribution through overexpression of ADF. After that, pterostilbene effectively inhibited the expression of MMP-9 and the degradation of BM components by activating the Wnt pathway, thereby further protecting the BBB and contributing to its long-term protective effect. Pterostilbene treatment co-protects the BBB by regulating cytoskeletal rearrangement and BM degradation in BMECs.

Author contributions

Z. H. Y. and Y. J. L. conceptualized and designed the research; Z. H. Y. provided the financial support; Y. J. L., W. K. B. and L. J. L. mainly participated in the pharmacological experiments *in vivo*; Y. J. L. and W. K. B. performed the mechanism research *in vitro*; Y. Y. Y., H. B. L., B. Y. Z., A. L. L. and Z. Y. H. provided the computer-aided methodology; Y. J. L., J. L. and X. C. contributed to the acquisition and analysis of data; Y. J. L. and Z. H. Y. obtained resources and wrote the original draft; Y. Y. Y. and W. K. B. conducted a thorough review and editing of the manuscript to enhance its quality. All authors read and approved the paper.

Conflicts of interest

The authors declare that they have no known competing financial interests or personal relationships that could have appeared to influence the work reported in this paper.

Acknowledgements

This study was supported by the National Natural Science Foundation of China (No. 81973744 and 81473579), the CAMS Innovation Fund for Medical Science (CIFMS) (No. 2022-I2M-1-018 and 2022-I2M-2-001), Beijing Science and Technology Programme (No. Z221100003522009), and the Beijing Natural Science Foundation (No. 7173267).

All animal procedures were performed in accordance with the Guidelines for Care and Use of Laboratory Animals of Institute of medicinal plants, Chinese Academy of Medical Sciences and approved by the Animal Ethics Committee of Institute of Medicinal Plant Development, Chinese Academy of Medical Sciences.

References

1 M. Zhou, H. Wang, X. Zeng, P. Yin, J. Zhu, W. Chen, X. Li, L. Wang, L. Wang, Y. Liu, *et al.*, Mortality, morbidity, and risk factors in China and its provinces, 1990–2017: a systematic analysis for the Global Burden of Disease Study 2017, *Lancet*, 2019, **394**, 1145–1158.

2 E. J. Benjamin, P. Muntner, A. Alonso, M. S. Bittencourt, C. W. Callaway, A. P. Carson, A. M. Chamberlain, A. R. Chang, S. Cheng, S. R. Das, *et al.*, Heart Disease and Stroke Statistics-2019 Update: A Report From the American Heart Association, *Circulation*, 2019, **139**, e56–e528.

3 M. Yepes, B. D. Roussel, C. Ali and D. Vivien, Tissue-type plasminogen activator in the ischemic brain: more than a thrombolytic, *Trends Neurosci.*, 2009, **32**, 48–55.

4 Z. Zhou, J. Lu, W. W. Liu, A. Manaenko, X. Hou, Q. Mei, J. L. Huang, J. Tang, J. H. Zhang, H. Yao, *et al.*, Advances in stroke pharmacology, *Pharmacol. Ther.*, 2018, **191**, 23–42.

5 H. Amani, R. Habibey, F. Shokri, S. J. Hajmiresmail, O. Akhavan, A. Mashaghi and H. Pazoki-Toroudi, Selenium nanoparticles for targeted stroke therapy through modulation of inflammatory and metabolic signaling, *Sci. Rep.*, 2019, **9**, 6044.
6 R. Brouns and P. P. De Deyn, The complexity of neurobiological processes in acute ischemic stroke, *Clin. Neurol. Neurosurg.*, 2009, **111**, 483–495.
7 L. Olah, S. Wecker and M. Hoehn, Secondary deterioration of apparent diffusion coefficient after 1-hour transient focal cerebral ischemia in rats, *J. Cereb. Blood Flow Metab.*, 2000, **20**, 1474–1482.
8 Y. Wallez and P. Huber, Endothelial adherens and tight junctions in vascular homeostasis, inflammation and angiogenesis, *Biochim. Biophys. Acta*, 2008, **1778**, 794–809.
9 H. J. Choi, N. E. Kim, J. Kim, S. An, S. H. Yang, J. Ha, S. Cho, I. Kwon, Y. D. Kim, H. S. Nam, *et al.*, Dabigatran reduces endothelial permeability through inhibition of thrombin-induced cytoskeleton reorganization, *Thromb. Res.*, 2018, **167**, 165–171.
10 A. Manaenko, P. Yang, D. Nowrangi, E. Budbazar, R. E. Hartman, A. Obenaus, W. J. Pearce, J. H. Zhang and J. Tang, Inhibition of stress fiber formation preserves blood-brain barrier after intracerebral hemorrhage in mice, *J. Cereb. Blood Flow Metab.*, 2018, **38**, 87–102.
11 E. Vandenbroucke, D. Mehta, R. Minshall and A. B. Malik, Regulation of endothelial junctional permeability, *Ann. N. Y. Acad. Sci.*, 2008, **1123**, 134–145.
12 Y. Yang and G. A. Rosenberg, Matrix metalloproteinases as therapeutic targets for stroke, *Brain Res.*, 2015, **1623**, 30–38.
13 M. Reis and S. Liebner, Wnt signaling in the vasculature, *Exp. Cell Res.*, 2013, **319**, 1317–1323.
14 K. A. Tran, X. Zhang, D. Predescu, X. Huang, R. F. Machado, J. R. Gothert, A. B. Malik, T. Valyi-Nagy and Y. Y. Zhao, Endothelial beta-Catenin Signaling Is Required for Maintaining Adult Blood-Brain Barrier Integrity and Central Nervous System Homeostasis, *Circulation*, 2016, **133**, 177–186.
15 C. Artus, F. Glacial, K. Ganeshamoorthy, N. Ziegler, M. Godet, T. Guilbert, S. Liebner and P. O. Couraud, The Wnt/planar cell polarity signaling pathway contributes to the integrity of tight junctions in brain endothelial cells, *J. Cereb. Blood Flow Metab.*, 2014, **34**, 433–440.
16 N. Ziegler, K. Awwad, B. Fisslthaler, M. Reis, K. Devraj, M. Corada, S. P. Minardi, E. Dejana, K. H. Plate, I. Fleming, *et al.*, beta-Catenin Is Required for Endothelial Cyp1b1 Regulation Influencing Metabolic Barrier Function, *J. Neurosci.*, 2016, **36**, 8921–8935.
17 S. Liebner, M. Corada, T. Bangsow, J. Babbage, A. Taddei, C. J. Czupalla, M. Reis, A. Felici, H. Wolburg, M. Fruttiger, *et al.*, Wnt/beta-catenin signaling controls development of the blood-brain barrier, *J. Cell Biol.*, 2008, **183**, 409–417.
18 Y. Wang, Y. Xu, Q. Liu, Y. Zhang, Z. Gao, M. Yin, N. Jiang, G. Cao, B. Yu, Z. Cao, *et al.*, Myosin IIA-related Actomyosin Contractility Mediates Oxidative Stress-induced Neuronal Apoptosis, *Front. Mol. Neurosci.*, 2017, **10**, 75.
19 P. Polakis, Formation of the blood-brain barrier: Wnt signaling seals the deal, *J. Cell Biol.*, 2008, **183**, 371–373.
20 X. Fan, W. Shen, L. Wang and Y. Zhang, Efficacy and Safety of DL-3-n-Butylphthalide in the Treatment of Poststroke Cognitive Impairment: A Systematic Review and Meta-Analysis, *Front. Pharmacol.*, 2021, **12**, 810297.
21 T. Zhang, W. Jia and X. Sun, 3-n-Butylphthalide (NBP) reduces apoptosis and enhances vascular endothelial growth factor (VEGF) up-regulation in diabetic rats, *Neurol. Res.*, 2010, **32**, 390–396.
22 J. Wang, Y. Li, H. Yu, G. Li, S. Bai, S. Chen, P. Zhang and Z. Tang, Dl-3-N-Butylphthalide Promotes Angiogenesis in an Optimized Model of Transient Ischemic Attack in C57BL/6 Mice, *Front. Pharmacol.*, 2021, **12**, 751397.
23 I. Alquisiras-Burgos, A. Ortiz-Plata, J. Franco-Perez, A. Millan and P. Aguilera, Resveratrol reduces cerebral edema through inhibition of de novo SUR1 expression induced after focal ischemia, *Exp. Neurol.*, 2020, **330**, 113353.
24 X. Lu, J. Dong, D. Zheng, X. Li, D. Ding and H. Xu, Reperfusion combined with intraarterial administration of resveratrol-loaded nanoparticles improved cerebral ischemia-reperfusion injury in rats, *Nanomedicine*, 2020, **28**, 102208.
25 N. Pineda-Ramirez, I. Alquisiras-Burgos, A. Ortiz-Plata, M. E. Ruiz-Tachiquin, M. Espinoza-Rojo and P. Aguilera, Resveratrol Activates Neuronal Autophagy Through AMPK in the Ischemic Brain, *Mol. Neurobiol.*, 2020, **57**, 1055–1069.
26 J. Meng, Y. Chen, F. Bi, H. Li, C. Chang and W. Liu, Pterostilbene attenuates amyloid-β induced neurotoxicity with regulating PDE4A-CREB-BDNF pathway, *Am. J. Transl. Res.*, 2019, **11**, 6356–6369.
27 H. S. Aiyer, A. M. Warri, D. R. Woode, L. Hilakivi-Clarke and R. Clarke, Influence of berry polyphenols on receptor signaling and cell-death pathways: implications for breast cancer prevention, *J. Agric. Food Chem.*, 2012, **60**, 5693–5708.
28 L. Bavaresco, C. Fregoni, E. Cantù and M. Trevisan, Stilbene compounds: from the grapevine to wine, *Drugs Exp. Clin. Res.*, 1999, **25**, 57–63.
29 A. Rimando, W. Kalt, J. Magee, J. Dewey and J. Ballington, Resveratrol, pterostilbene, and piceatannol in vaccinium berries, *J. Agric. Food Chem.*, 2004, **52**, 4713–4719.
30 P. Rodríguez-Bonilla, J. López-Nicolás, L. Méndez-Cazorla and F. García-Carmona, Development of a reversed phase high performance liquid chromatography method based on the use of cyclodextrins as mobile phase additives to determine pterostilbene in blueberries, *J. Chromatogr. B: Anal. Technol. Biomed. Life Sci.*, 2011, **879**, 1091–1097.
31 J. Liu, C. Fan, L. Yu, Y. Yang, S. Jiang, Z. Ma, W. Hu, T. Li, Z. Yang, T. Tian, *et al.*, Pterostilbene exerts an anti-inflammatory effect via regulating endoplasmic reticulum stress in endothelial cells, *Cytokine*, 2016, **77**, 88–97.
32 C. L. Hsu, Y. J. Lin, C. T. Ho and G. C. Yen, The inhibitory effect of pterostilbene on inflammatory responses during

the interaction of 3T3-L1 adipocytes and RAW 264.7 macrophages, *J. Agric. Food Chem.*, 2013, **61**, 602–610.

33 B. Elango, S. Dornadula, R. Paulmurugan and K. M. Ramkumar, Pterostilbene Ameliorates Streptozotocin-Induced Diabetes through Enhancing Antioxidant Signaling Pathways Mediated by Nrf2, *Chem. Res. Toxicol.*, 2016, **29**, 47–57.

34 J. Acharya and S. Ghaskadbi, Protective effect of Pterostilbene against free radical mediated oxidative damage, *BMC Complement. Altern. Med.*, 2013, **13**, 238.

35 Z. Ma, X. Zhang, L. Xu, D. Liu, S. Di, W. Li, J. Zhang, H. Zhang, X. Li, J. Han, *et al.*, Pterostilbene: Mechanisms of its action as oncostatic agent in cell models and in vivo studies, *Pharmacol. Res.*, 2019, **145**, 104265.

36 S. Paul, A. M. Rimando, H. J. Lee, Y. Ji, B. S. Reddy and N. Suh, Anti-inflammatory action of pterostilbene is mediated through the p38 mitogen-activated protein kinase pathway in colon cancer cells, *Cancer Prev. Res.*, 2009, **2**, 650–657.

37 D. McCormack and D. McFadden, Pterostilbene and cancer: current review, *J. Surg. Res.*, 2012, **173**, e53–e61.

38 Y. R. Li, S. Li and C. C. Lin, Effect of resveratrol and pterostilbene on aging and longevity, *BioFactors*, 2018, **44**, 69–82.

39 P. Penalver, S. Zodio, R. Lucas, M. V. de-Paz and J. C. Morales, Neuroprotective and Anti-inflammatory Effects of Pterostilbene Metabolites in Human Neuroblastoma SH-SY5Y and RAW 264.7 Macrophage Cells, *J. Agric. Food Chem.*, 2020, **68**, 1609–1620.

40 J. Chang, A. Rimando, M. Pallas, A. Camins, D. Porquet, J. Reeves, B. Shukitt-Hale, M. Smith, J. Joseph and G. Casadesus, Low-dose pterostilbene, but not resveratrol, is a potent neuromodulator in aging and Alzheimer's disease, *Neurobiol. Aging*, 2012, **33**, 2062–2071.

41 L. Aguirre, S. Palacios-Ortega, A. Fernandez-Quintela, E. Hijona, L. Bujanda and M. P. Portillo, Pterostilbene Reduces Liver Steatosis and Modifies Hepatic Fatty Acid Profile in Obese Rats, *Nutrients*, 2019, **11**, 961.

42 M. H. Pan, J. C. Wu, C. T. Ho and C. S. Lai, Antiobesity molecular mechanisms of action: Resveratrol and pterostilbene, *BioFactors*, 2018, **44**, 50–60.

43 S. Gomez-Zorita, A. Fernandez-Quintela, A. Lasa, L. Aguirre, A. M. Rimando and M. P. Portillo, Pterostilbene, a dimethyl ether derivative of resveratrol, reduces fat accumulation in rats fed an obesogenic diet, *J. Agric. Food Chem.*, 2014, **62**, 8371–8378.

44 R. Kosuru and S. Singh, Pterostilbene ameliorates insulin sensitivity, glycemic control and oxidative stress in fructose-fed diabetic rats, *Life Sci.*, 2017, **182**, 112–121.

45 H. Sun, X. Liu, S. R. Long, W. Teng, H. Ge, Y. Wang, S. Yu, Y. Xue, Y. Zhang, X. Li, *et al.*, Antidiabetic effects of pterostilbene through PI3K/Akt signal pathway in high fat diet and STZ-induced diabetic rats, *Eur. J. Pharmacol.*, 2019, **859**, 172526.

46 H. Y. Tsai, C. T. Ho and Y. K. Chen, Biological actions and molecular effects of resveratrol, pterostilbene, and 3′-hydroxypterostilbene, *J. Food Drug Anal.*, 2017, **25**, 134–147.

47 Y. Liu, Y. You, J. Lu, X. Chen and Z. Yang, Recent Advances in Synthesis, Bioactivity, and Pharmacokinetics of Pterostilbene, an Important Analog of Resveratrol, *Molecules*, 2020, **25**, 5166.

48 Y. Liu and Z. Yang, Research progress on pharmacological effects and mechanism of Pterostilbene in the treatment of cerebral ischemia, *Pharmacol. Clin. Chin. Mater. Med.*, 2021, **37**, 210–215.

49 H. Liang, N. Matei, D. W. McBride, Y. Xu, J. Tang, B. Luo and J. H. Zhang, Activation of TGR5 protects blood brain barrier via the BRCA1/Sirt1 pathway after middle cerebral artery occlusion in rats, *J. Biomed. Sci.*, 2020, **27**, 61.

50 M. Bieber, J. Gronewold, A. C. Scharf, M. K. Schuhmann, F. Langhauser, S. Hopp, S. Mencl, E. Geuss, J. Leinweber, J. Guthmann, *et al.*, Validity and Reliability of Neurological Scores in Mice Exposed to Middle Cerebral Artery Occlusion, *Stroke*, 2019, **50**, 2875–2882.

51 Y. Zheng, L. Kong, H. Jia, B. Zhang, Z. Wang, L. Xu, A. Liu and G. Du, Network pharmacology study on anti-stroke of Xiaoshuan Tongluo formula based on systematic compound-target interaction prediction models, *Acta Pharm. Sin.*, 2020, **55**, 256–264.

52 S. O. Bachurin, E. V. Bovina and A. A. Ustyugov, Drugs in Clinical Trials for Alzheimer's Disease: The Major Trends, *Med. Res. Rev.*, 2017, **37**, 1186–1225.

53 X. Chen, Z. Ji and Y. Chen, TTD: Therapeutic Target Database, *Nucleic Acids Res.*, 2002, **30**, 412–415.

54 G. Provan, P. Langley and P. Smyth, Bayesian network classifiers, *Mach. Learn.*, 1997, **29**, 131–163.

55 M. Stone, Cross-validation and multinomial prediction, *Biometrika*, 1974, **61**, 509–515.

56 D. Rogers, R. D. Brown and M. Hahn, Using extended-connectivity fingerprints with Laplacian-modified Bayesian analysis in high-throughput screening follow-up, *J. Biomol. Screening*, 2005, **10**, 682–686.

57 A. Cereto-Massague, M. J. Ojeda, C. Valls, M. Mulero, S. Garcia-Vallve and G. Pujadas, Molecular fingerprint similarity search in virtual screening, *Methods*, 2015, **71**, 58–63.

58 S. N. H. Bukhari, A. Jain, E. Haq, M. A. Khder, R. Neware, J. Bhola and M. L. Najafi, Machine Learning-Based Ensemble Model for Zika Virus T-Cell Epitope Prediction, *J. Healthc. Eng.*, 2021, **2021**, 9591670.

59 W. Zhao, J. Zou, Y. Jiang, G. Ma and Q. Yu, Influence of Magnesium Ion on Molecular Docking Based on HPPK, *Acta Chim. Sin.*, 2005, **63**, 434–438.

60 S. Pellegrin and H. Mellor, Actin stress fibres, *J. Cell Sci.*, 2007, **120**, 3491–3499.

61 J. Bogousslavsky, G. Van Melle and F. Regli, The Lausanne Stroke Registry analysis of 1,000 consecutive patients with first stroke, *Stroke*, 1988, **19**, 1083–1092.

62 I. L. Gubskiy, D. D. Namestnikova, E. A. Cherkashova, V. P. Chekhonin, V. P. Baklaushev, L. V. Gubsky and K. N. Yarygin, MRI Guiding of the Middle Cerebral Artery Occlusion in Rats Aimed to Improve Stroke Modeling, *Transl. Stroke Res.*, 2018, **9**, 417–425.

63 A. A. Neuhaus, Y. Couch, G. Hadley and A. M. Buchan, Neuroprotection in stroke: the importance of collaboration and reproducibility, *Brain*, 2017, **140**, 2079–2092.
64 F. Fluri, M. K. Schuhmann and C. Kleinschnitz, Animal models of ischemic stroke and their application in clinical research, *Drug Des., Dev. Ther.*, 2015, **9**, 3445–3454.
65 L. Kaplan, B. W. Chow and C. Gu, Neuronal regulation of the blood-brain barrier and neurovascular coupling, *Nat. Rev. Neurosci.*, 2020, **21**, 416–432.
66 R. Khatri, A. McKinney, B. Swenson and V. Janardhan, Blood-brain barrier, reperfusion injury, and hemorrhagic transformation in acute ischemic stroke, *Neurology*, 2012, **79**, S52–S57.
67 J. Keaney and M. Campbell, The dynamic blood-brain barrier, *FEBS J.*, 2015, **282**, 4067–4079.
68 S. Nag, A. Kapadia and D. J. Stewart, Review: molecular pathogenesis of blood-brain barrier breakdown in acute brain injury, *Neuropathol. Appl. Neurobiol.*, 2011, **37**, 3–23.
69 P. Guo, Z. Jin, H. Wu, X. Li, J. Ke, Z. Zhang and Q. Zhao, Effects of irisin on the dysfunction of blood-brain barrier in rats after focal cerebral ischemia/reperfusion, *Brain Behav.*, 2019, **9**, e01425.
70 M. B. Liu, W. Wang, J. M. Gao, F. Li, J. S. Shi and Q. H. Gong, Icariside II attenuates cerebral ischemia/reperfusion-induced blood-brain barrier dysfunction in rats via regulating the balance of MMP9/TIMP1, *Acta Pharmacol. Sin.*, 2020, **41**, 1547–1556.
71 H. Chen, Y. Luo, B. Tsoi, B. Gu, S. Qi and J. Shen, Angong Niuhuang Wan reduces hemorrhagic transformation and mortality in ischemic stroke rats with delayed thrombolysis: involvement of peroxynitrite-mediated MMP-9 activation, *Chin. Med.*, 2022, **17**, 51.
72 Y. Shi, L. Zhang, H. Pu, L. Mao, X. Hu, X. Jiang, N. Xu, R. A. Stetler, F. Zhang, X. Liu, *et al.*, Rapid endothelial cytoskeletal reorganization enables early blood-brain barrier disruption and long-term ischaemic reperfusion brain injury, *Nat. Commun.*, 2016, **7**, 10523.
73 W. Zhang and S. J. Gunst, Non-muscle (NM) myosin heavy chain phosphorylation regulates the formation of NM myosin filaments, adhesome assembly and smooth muscle contraction, *J. Physiol.*, 2017, **595**, 4279–4300.
74 K. W. Wu, L. L. Lv, Y. Lei, C. Qian and F. Y. Sun, Endothelial cells promote excitatory synaptogenesis and improve ischemia-induced motor deficits in neonatal mice, *Neurobiol. Dis.*, 2019, **121**, 230–239.
75 S. M. Stamatovic, R. F. Keep, M. M. Wang, I. Jankovic and A. V. Andjelkovic, Caveolae-mediated internalization of occludin and claudin-5 during CCL2-induced tight junction remodeling in brain endothelial cells, *J. Biol. Chem.*, 2009, **284**, 19053–19066.
76 N. Prasain and T. Stevens, The actin cytoskeleton in endothelial cell phenotypes, *Microvasc. Res.*, 2009, **77**, 53–63.
77 M. V. Suurna, S. L. Ashworth, M. Hosford, R. M. Sandoval, S. E. Wean, B. M. Shah, J. R. Bamburg and B. A. Molitoris, Cofilin mediates ATP depletion-induced endothelial cell actin alterations, *Am. J. Physiol-Renal*, 2006, **290**, F1398–F1407.
78 J. Banmburg and O. Wiggan, ADF/cofilin and actin dynamics in disease, *Trends Cell Biol.*, 2002, **12**, 598–605.
79 C. Qin, P. Zhou, L. Wang, M. Mamtilahun, W. Li, Z. Zhang, G. Y. Yang and Y. Wang, Dl-3-N-butylphthalide attenuates ischemic reperfusion injury by improving the function of cerebral artery and circulation, *J. Cereb. Blood Flow Metab.*, 2019, **39**, 2011–2021.
80 C. S. Yang, A. Guo, Y. Li, K. Shi, F. D. Shi and M. Li, Dl-3-n-butylphthalide Reduces Neurovascular Inflammation and Ischemic Brain Injury in Mice, *Aging Dis.*, 2019, **10**, 964–976.
81 F. Li, Q. Ma, H. Zhao, R. Wang, Z. Tao, Z. Fan, S. Zhang, G. Li and Y. Luo, L-3-n-Butylphthalide reduces ischemic stroke injury and increases M2 microglial polarization, *Metab. Brain Dis.*, 2018, **33**, 1995–2003.
82 A. Chakraborty, N. Gupta, K. Ghosh and P. Roy, In vitro evaluation of the cytotoxic, anti-proliferative and anti-oxidant properties of pterostilbene isolated from Pterocarpus marsupium, *Toxicol. in Vitro*, 2010, **24**, 1215–1228.
83 C. He, C. P. Tsipis, J. C. LaManna and K. Xu, Environmental Enrichment Induces Increased Cerebral Capillary Density and Improved Cognitive Function in Mice, *Adv. Exp. Med. Biol.*, 2017, **977**, 175–181.
84 Y. B. Ji, Q. Gao, X. X. Tan, X. W. Huang, Y. Z. Ma, C. Fang, S. N. Wang, L. H. Qiu, Y. X. Cheng, F. Y. Guo, *et al.*, Lithium alleviates blood-brain barrier breakdown after cerebral ischemia and reperfusion by upregulating endothelial Wnt/beta-catenin signaling in mice, *Neuropharmacology*, 2021, **186**, 108474.
85 J. Yu, Q. Liu, X. Li, M. Zhao, T. Sun, N. Hu, W. Jiang, R. Zhang, P. Yang and Q. Yang, Oxymatrine improves blood-brain barrier integrity after cerebral ischemia-reperfusion injury by downregulating CAV1 and MMP9 expression, *Phytomedicine*, 2021, **84**, 153505.
86 C. Iadecola and J. Anrather, Stroke research at a crossroad: asking the brain for directions, *Nat. Neurosci.*, 2011, **14**, 1363–1368.

